

Multi-step Inertial Accelerated Doubly Stochastic Gradient Methods for Block Term Tensor Decomposition

Zehui Liu*, Qingsong Wang†, Chunfeng Cui‡

January 10, 2025

Abstract

In this paper, we explore a specific optimization problem that combines a differentiable non-convex function with a nondifferentiable function for multi-block variables, which is particularly relevant to tackle the multilinear rank- $(L_r, L_r, 1)$ block-term tensor decomposition model with a regularization term. While existing algorithms often suffer from high per-iteration complexity and slow convergence, this paper employs a unified multi-step inertial accelerated doubly stochastic gradient descent method tailored for structured rank- $(L_r, L_r, 1)$ tensor decomposition, referred to as Midas-LL1. We also introduce an extended multi-step variance-reduced stochastic estimator framework. Our analysis under this new framework demonstrates the subsequential and sequential convergence of the proposed algorithm under certain conditions and illustrates the sublinear convergence rate of the subsequence, showing that the Midas-LL1 algorithm requires at most $\mathcal{O}(\varepsilon^{-2})$ iterations in expectation to reach an ε -stationary point. The proposed algorithm is evaluated on several datasets, and the results indicate that Midas-LL1 outperforms existing state-of-the-art algorithms in terms of both computational speed and solution quality.

Keywords: Block term tensor decomposition, multi-step inertial acceleration, stochastic gradient descent, variance-reduced estimator, nonconvex and nonsmooth model.

1 Introduction

In this paper, we focus on solving the composite optimization problem for multi-block variables, formulated as follows:

$$\min_{\{x_n\}_{n=1}^N} \Phi(x_1, \dots, x_N) \equiv f(x_1, \dots, x_N) + \sum_{n=1}^N h_n(x_n), \quad (1)$$

where $x_n \in \mathbb{R}^{d_n}$, $f: \prod_{n=1}^N \mathbb{R}^{d_n} \rightarrow \mathbb{R}$ is a continuously differentiable nonconvex function for the entire variable set $x = (x_1, \dots, x_N)$, and convex concerning each block x_n when the other blocks are fixed, i.e., f is a block multiconvex function. The function $f(x)$ has a finite-sum structure, expressed as $f(x) = \frac{1}{n} \sum_{i=1}^n f_i(x)$, and h_n for $n = 1, \dots, N$, are extended-value convex functions that serve

*LMIB, School of Mathematical Sciences, Beihang University, Beijing 100191, China. Email: liuzehui@buaa.edu.cn

†School of Mathematics and Computational Science, Xiangtan University, Xiangtan 411105, China. Email: nothing2wang@hotmail.com

‡LMIB, School of Mathematical Sciences, Beihang University, Beijing 100191, China. Email: chunfengcui@buaa.edu.cn

as regularization terms, capturing prior information about x_n , such as non-negativity [28]. We consider a class of problems that are nonsmooth and nonconvex. Optimization problems of the form (1) are particularly relevant in practical applications and are widely used across various fields of science and engineering, including blind source separation [22], nonnegative matrix and tensor factorization [5, 6, 23, 46], and Poisson inverse problems [4].

Several methods have been developed to tackle these types of optimization problems. One state-of-the-art approach is the block coordinate descent (BCD) [39] method of Gauss-Seidel type, which iteratively optimizes each block of variables while keeping the others fixed, effectively breaking down a complex problem into simpler subproblems. Additionally, BCD allows these blocks to be updated via proximal minimization, as discussed in [1]. However, it is important to note that both BCD and proximal BCD schemes generally involve an inner minimization problem. This can lead to a higher computational burden, particularly when the minimizer does not have a closed-form solution. In 2013, Xu and Yin [48] proposed an efficient proximal linearized BCD approach, which leverages the linearization of the differentiable component function f , facilitating the development of efficient numerical algorithms. Bolte, Sabach, and Teboulle [3] proposed the proximal alternating linearized minimization (PALM) for blocks $N \geq 2$, where the blocks are taken in cyclic order while fixing the previously computed iterate. The proximal linearized BCD/PALM is briefly outlined below:

$$\mathbf{x}_n^{k+1} = \operatorname{argmin}_{\mathbf{x}_n \in \mathbb{R}^{d_n}} \langle \nabla f_n^{k+1}(\mathbf{x}_n), \mathbf{x}_n - \mathbf{x}_n^k \rangle + \frac{1}{2\eta^k} \|\mathbf{x}_n - \mathbf{x}_n^k\|^2 + h_n(\mathbf{x}_n), \quad (2)$$

where $f_n^{k+1}(\mathbf{x}_n) \triangleq f(\mathbf{x}_1^{k+1}, \dots, \mathbf{x}_{n-1}^{k+1}, \mathbf{x}_n, \mathbf{x}_{n+1}^k, \dots, \mathbf{x}_N^k)$ for all n , and the stepsize η^k is computed according to Lipschitz constants of $\nabla f_n^{k+1}(\mathbf{x}_n)$. Based on the Kurdyka-Lojasiewicz inequality, the bounded sequence $\{\mathbf{x}_1^k, \dots, \mathbf{x}_N^k\}_{k=0}^\infty$ generated by (2) can converge globally to the critical point of (1).

Stochastic algorithms can reduce iteration costs when the data dimension is large. Xu and Yin [49] integrated a vanilla stochastic gradient descent (SGD) estimator with PALM, and Driggs et al. [12] introduced the SPRING algorithm, a stochastic version of PALM, using more sophisticated variance-reduced gradient estimators instead of the vanilla stochastic gradient descent estimators. Additionally, Hertrich and Steidl [18] proposed a stochastic version of iPALM [34] that introduced an inertial step to improve the performance of PALM further, and established its convergence under similar conditions. Liang et al. [27] introduced a multi-step inertial forward-backward splitting algorithm aimed at minimizing the sum of two non-necessarily convex functions. Furthermore, Guo et al. [17] developed a stochastic two-step inertial Bregman PALM algorithm for large-scale nonconvex and nonsmooth optimization problems.

These advancements in stochastic algorithms are particularly relevant for high-dimensional data problems. Specifically, the form of problem (1) can be effectively applied to tensor decomposition [23] with regularization. Tensor decompositions generalize matrix decompositions and are powerful tools that enable the recovery of underlying components. BCD and tensor decomposition are linked together through the matrix unfolding operation, rearranging the elements of a tensor to a matrix and pushing the latent factors to the rightmost position in the unfolded tensor representation. In 2020, Fu et al. [14] proposed BrasCPD, a block-randomized stochastic algorithmic framework for computing the CP decomposition [19] of large-scale dense tensors. Wang et al. introduced mBrasCPD [43] and iBrasCPD [45], which accelerate the SGD scheme using the heavy ball method [35] and inertial acceleration, respectively. Additionally, Pu et al. [36] developed a block-randomized stochastic mirror descent (SMD) algorithmic framework for large-scale generalized CP decomposition (GCP) [21]. Recently, Liu et al. [30] developed an inertial accelerated version of SMD for GCP problem, and showed sub-sequential and sequentially convergence guarantees. Besides CP decomposition, many tensor factorization models, such as Tucker decomposition [40–42] and block term decomposition (BTD) [7–9], exhibit similar multi-linearity properties in their respective unfolded forms. However, the aforementioned algorithms primarily focus on solving CP decomposition

problems, with limited attention given to other types of tensor decomposition problems.

CP decomposition and Tucker decomposition correspond to different tensor generalizations of matrix rank. Tucker decomposition is associated with n -ranks, generalizing column and row ranks. In contrast, CP decomposition defines rank as the minimal number of rank-1 terms required to represent a tensor, treating all tensor modes equally and processing them identically. However, Tucker decomposition does not explicitly divide a tensor into a sum of component tensors, complicating its direct application to the linear mixture model. In 2008, the Tucker and CP decompositions were connected by introducing the BTD. This model overcomes the CP decomposition limitation that each component must be rank-1 and the Tucker decomposition constraint of having a single component tensor. Consequently, BTD has found extensive application in hyperspectral unmixing [2, 31], and community detection in networks [16]. In [8], BTD was introduced as a sum of R rank- (L_r, M_r, N_r) terms ($r = 1, 2, \dots, R$) in general. Domanov et al. [11] recently presented new deterministic and generic conditions for the uniqueness of rank- (L_r, M_r, N_r) decompositions. Another special case of rank- $(L_r, L_r, 1)$ BTD for third-order tensor has attracted more attention, because of both its more frequent occurrence in applications and the existence of more concrete and easier to check uniqueness conditions. For instance, a hyperspectral image (HSI) can be represented as a third-order tensor, where its modes are distinguishable in a spectral-spatial manner, with two spatial modes separate from a spectral mode. Therefore, rank- $(L_r, L_r, 1)$ BTD is a suitable model, where the first two modes correspond to the spatial positions, and the third mode corresponds to the spectral information. This paper shall also focus on this specific and widely-used rank- $(L_r, L_r, 1)$ BTD model.

The rank- $(L_r, L_r, 1)$ BTD often have structural constraints and regularization on the latent factors, which usually come from physical meaning and prior information on HSIs. Designing tailored algorithms for structured rank- $(L_r, L_r, 1)$ tensor decomposition presents several challenges. One key issue is that the speed of existing methods is often inadequate. For example, Alternating Least Squares (ALS) has been extended to compute tensor BTD as described in [9]. However, the primary bottleneck in ALS lies in the matricized-tensor times Khatri-Rao product (MTTKRP) [13], which becomes even more computationally demanding in the BTD context compared to its application in CP decomposition. This increased computational cost arises because two of the latent factors in BTD are typically larger in scale. Nonnegativity constraints on the latent factors are typically managed by the classic multiplicative update (MU) algorithm [26], which updates one factor using the majorization-minimization method but with a conservative stepsize. The MU algorithm is also prone to numerical issues in some cases, when there are iterates that contain zero elements [29]. In addition, the ALS-MU [15, 37, 47] combination often leads to a considerably high per-iteration complexity. These algorithms, however, also encounter challenges related to slow convergence issues. These limitations remain a critical area for ongoing research, prompting us to explore the potential of stochastic methods in computing rank- $(L_r, L_r, 1)$ BTD.

In this paper, a doubly stochastic gradient descent method with multi-step inertial acceleration is proposed to tackle the nonconvex and nonsmooth optimization problem (1). This method is particularly suitable for applications in rank- $(L_r, L_r, 1)$ BTD. Our detailed contributions are as follows:

- (i) We introduce a multi-step inertial accelerated block-randomized stochastic gradient descent method, i.e. doubly stochastic algorithm for rank- $(L_r, L_r, 1)$ block-term decomposition problem, denoted by Midas-LL1. Inherited from the variance-reduced stochastic estimator, we propose an extended multi-step and multi-block variance-reduced stochastic estimator. Based on these, we demonstrate that Midas-LL1 achieves a sublinear convergence rate for the generated subsequence.
- (ii) The global convergence of the sequence generated by Midas-LL1 is established. We introduce a novel multi-step Lyapunov function, showing that the algorithm requires at most $\mathcal{O}(\varepsilon^{-2})$

iterations in expectation to attain an ε -stationary point.

- (iii) We conduct extensive experiments on two hyperspectral image datasets and two video datasets to illustrate the effectiveness of our proposed Midas-LL1 algorithms. Our numerical results indicate that incorporating variance-reduced stochastic gradient estimators and multi-step acceleration into Midas-LL1 yields superior performance.

The rest of this paper is organized as follows. Section 2 provides the essential definitions and preliminary results related to existing models and algorithms. Section 3 introduces the formulation of the proposed Midas-LL1 algorithm. Section 4 focuses on establishing the convergence properties and convergence rate of Midas-LL1. In Section 5, we evaluate the performance of the Midas-LL1 algorithm in comparison with several baseline methods using real-world datasets. Finally, the paper concludes in Section 6.

2 Preliminaries

In this section, we summarize some useful definitions and introduce the block term decomposition as well as various stochastic methods for tensor decomposition.

Definition 1. [38] Let $h : \mathbb{R}^d \rightarrow (-\infty, +\infty]$ be a proper and lower semicontinuous function. For $x \in \text{dom } h$, the Fréchet subdifferential of Φ at x , written $\hat{\partial}h(x)$, is the set of vectors $v \in \mathbb{R}^d$ which satisfy

$$\liminf_{y \rightarrow x} \frac{1}{\|x - y\|_2} [h(y) - h(x) - \langle v, y - x \rangle] \geq 0.$$

If $x \notin \text{dom } h$, then $\hat{\partial}h(x) = \emptyset$. The limiting subdifferential of h at $x \in \text{dom } h$, written $\partial h(x)$, is defined as follows:

$$\partial h(x) := \left\{ v \in \mathbb{R}^d : \exists x_k \rightarrow x, h(x_k) \rightarrow h(x), v_k \in \hat{\partial}h(x_k), v_k \rightarrow v \right\}.$$

Proposition 1. For all $(x_1, \dots, x_s) \in \text{dom } \Phi$ in problem (1) we have

$$\partial\Phi(\mathbf{x}) = \{\nabla_{\mathbf{x}_1} f(\mathbf{x}) + \partial h_1(\mathbf{x}_1)\} \times \dots \times \{\nabla_{\mathbf{x}_s} f(\mathbf{x}) + \partial h_s(\mathbf{x}_s)\}.$$

Proof. Observe first that we can get $\partial\Phi(\mathbf{x}) = \nabla f(\mathbf{x}) + \partial(\sum_{n=1}^s h_n)$, since f is continuously differentiable. Further, the subdifferential calculus for separable functions yields $\partial(\sum_{n=1}^s h_n) = \partial h_1(\mathbf{x}_1) \times \dots \times \partial h_s(\mathbf{x}_s)$. Hence we get the above equality. \square

Definition 2. ([25] ε -stationary point) Given $\varepsilon > 0$, a solution $\{x_1^*, \dots, x_s^*\}$ is said to be an ε -stationary point of function $\Phi(x_1, \dots, x_s)$ if

$$\text{dist}(0, \partial\Phi(x_1^*, \dots, x_s^*)) \leq \varepsilon.$$

2.1 Block term decomposition with rank- $(L_r, L_r, \mathbf{1})$

Tensor decomposition [23] can break a large-size tensor into many small-size factors, including CP [19, 20] and Tucker decomposition [40–42] connected with two different tensor generalizations of matrix decomposition. BTD [7–9] is proposed to unify the Tucker and CP, decomposing a tensor into a sum of low multilinear rank terms.

Consider an N -th order tensor $\mathcal{X} \in \mathbb{R}^{I_1 \times I_2 \times \dots \times I_N}$ with $\mathcal{X}(i_1, \dots, i_N)$ represents an element of \mathcal{X} . The block term decomposition is

$$\mathcal{X} = \sum_{r=1}^R \mathcal{G}_r \times_1 \mathbf{U}_r^{(1)} \times_2 \mathbf{U}_r^{(2)} \dots \times_N \mathbf{U}_r^{(N)}, \quad (3)$$

in which $\mathbf{U}_r^{(n)} \in \mathbb{R}^{I_n \times J_n^r}$ represents the n -th factor in the r -th term, and $\mathcal{G}_r \in \mathbb{R}_1^{J_1^r \times J_2^r \times \dots \times J_N^r}$ is the core tensor in the r -th term. If \mathcal{G}_r is an identity cubical tensor for all $r = 1, \dots, R$, then (3) becomes the CP decomposition. When $R = 1$, (3) reduces to Tucker decomposition. A visual representation of BTD for a third-order tensor is shown in Figure 1.

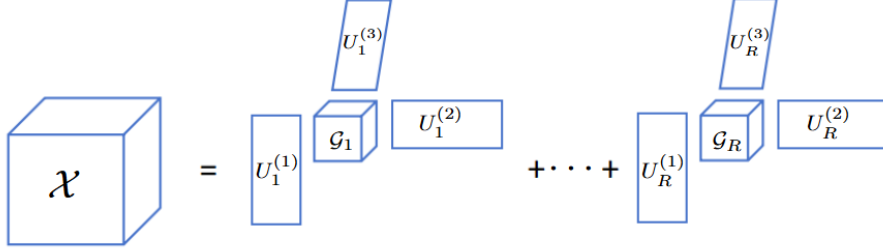


Figure 1: BTD for a third-order tensor.

The mode- n unfolding of \mathcal{X} , denoted by $X_{(n)}$, is a J_n -by- I_n matrix, where $J_n = \prod_{m=1, m \neq n}^N I_m$ and each element in $X_{(n)}$ is defined by

$$X_{(n)}(j, i_n) = \mathcal{X}(i_1, \dots, i_N),$$

where $j = 1 + \sum_{k=1, k \neq n}^N (i_k - 1) \bar{J}_k$ and $\bar{J}_k = \prod_{m=1, m \neq n}^{k-1} I_m$ [23]. A mode- n fiber is defined by fixing every index $(i_1, \dots, i_{n-1}, i_{n+1}, \dots, i_N)$ but keeping $i_n \in \{1, \dots, I_n\}$ in variation.

Under the umbrella of block term decomposition (3), the special case of BTD with rank- $(L_r, L_r, 1)$ terms has earned significant interest due to its frequently occurring application and the easily verifiable conditions for uniqueness. The BTD with rank- $(L_r, L_r, 1)$ approximates a third-order tensor as a sum of R component tensors, where each term is the outer product of a rank- L_r matrix and a vector. Specifically, let $A_1^r \in \mathbb{R}^{I_1 \times L_r}$ and $A_2^r \in \mathbb{R}^{I_2 \times L_r}$ be rank- L_r matrices, and $\mathbf{c}_r \in \mathbb{R}^{I_3}$ be a non-zero vector. Then, the rank- $(L_r, L_r, 1)$ BTD of $\mathcal{X} \in \mathbb{R}^{I_1 \times I_2 \times I_3}$ can be expressed as follows:

$$\mathcal{X} \approx \sum_{r=1}^R (A_{1,r} \cdot A_{2,r}^\top) \circ \mathbf{c}_r. \quad (4)$$

A visual representation of this decomposition for a third-order tensor is shown in Figure 2. The

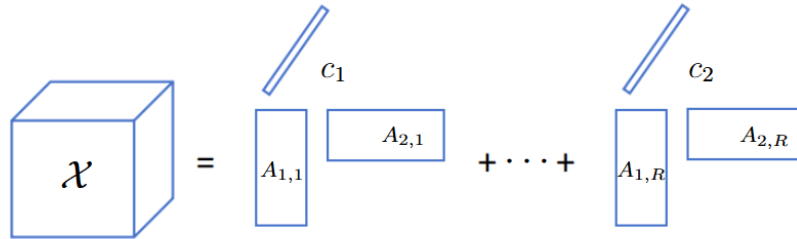


Figure 2: BTD with rank- $(L_r, L_r, 1)$ for a third-order tensor.

Canonical Polyadic Decomposition (CPD) becomes a specific case of BTD with rank- $(1, 1, 1)$ terms when $L_r = 1$. Consequently, permutation and scaling indeterminacies inherited from the CPD, a nice feature of this decomposition is that the rank-one block-terms $(A_1^r \cdot A_2^{r\top}) \circ \mathbf{c}_r$ are unique under

quite mild conditions. Therefore, the rank- $(L_r, L_r, 1)$ BTD is also called essentially unique when it is subject only to these trivial indeterminacies. We use the following interpretation to formulate (4) as the nonlinear least squares problem

$$f(A_1, A_2, A_3) = \frac{1}{2IN} \left\| \mathcal{X} - \sum_{r=1}^R (A_{1,r} \cdot A_{2,r}^\top) \circ \mathbf{c}_r \right\|_F^2, \quad (5)$$

where the partitioned matrices $A_1 = [A_{1,1}, \dots, A_{1,R}] \in \mathbb{R}^{I_1 \times \sum_{r=1}^R L_r}$, $A_2 = [A_2^1, \dots, A_2^R] \in \mathbb{R}^{I_2 \times \sum_{r=1}^R L_r}$, and $A_3 = [\mathbf{c}_1, \dots, \mathbf{c}_R] \in \mathbb{R}^{I_3 \times R}$. Denote $I = (I_1 I_2 I_3)^{\frac{1}{3}}$ as the geometric mean of the three dimensions. The function $f(\cdot)$ is smooth, yet it is both nonlinear and non-convex. The corresponding loss function is derived from a maximum likelihood estimate, predicated on the assumption that the data adhere to a Gaussian distribution. Alternative assumptions regarding the data distributions, such as those based on Bernoulli or Poisson distributions, would necessitate the formulation of distinct loss functions. For additional details, we refer the reader to [21].

By taking the structures of the variables A_n into consideration, we focus on the regularized problem as follows

$$\min_{\{A_n\}_{n=1}^3} \Phi(A_1, A_2, A_3) := f(A_1, A_2, A_3) + \sum_{n=1}^3 h_n(A_n). \quad (6)$$

Here, $h_n(A_n)$ denotes a structure promoting regularizer on A_n , such as column-wise orthogonality [24], Tikhonov regularization [33], nonnegativity [28]. Those regularizations may result in well-posed problems. For instance, if $A_n \in \mathbb{R}_+^{I_n \times R} := \{A_n | A_n \geq 0\}$ is applied, we can write $h_n(\cdot)$ as the indicator function:

$$h_n(A) = \mathcal{I}_{\mathbb{R}_+^{I_n \times R}}(A) = \begin{cases} 0, & A \geq 0, \\ \infty, & \text{otherwise.} \end{cases}$$

Suppose all factors but A_n are fixed, then (6) is reduced to the subproblem

$$\min_{A_n} \frac{1}{2IN} \|X_{(n)} - H_n A_n^\top\|_F^2 + h_n(A_n), \quad (7)$$

where H_n for $n = 1, 2$, and 3 is defined by

$$\begin{aligned} H_1 &= A_3 \circ_b A_2 = [c_1 \otimes A_2^1, \dots, c_R \otimes A_2^R] \in \mathbb{R}^{J_1 \times L}, \\ H_2 &= A_3 \circ_b A_1 = [c_1 \otimes A_1^1, \dots, c_R \otimes A_1^R] \in \mathbb{R}^{J_2 \times L}, \\ H_3 &= [(A_2^1 \circ A_1^1) 1_{L_1}, \dots, (A_2^R \circ A_1^R) 1_{L_R}] \in \mathbb{R}^{J_3 \times R}, \end{aligned} \quad (8)$$

where $L = \sum_{r=1}^R L_r$ and 1_{L_r} is all-one column vector with length L_r . The notation \circ_b is a generalized block-wise Khatri–Rao product for partitioned matrices with the same number of submatrices, which consists of the partition-wise Kronecker product. The formulation of H_3 is due to the last factor A_3 of BTD is the rank-1 component.

Optimization methods such as (proximal) gradient descent can solve the subproblem (7) directly. The gradient of f with respect to A_n is equal to

$$\nabla_{A_n} f(A_1, A_2, A_3) = \frac{1}{IN} (A_n H_n^\top H_n - X_{(n)}^\top H_n). \quad (9)$$

Computing $X_{(n)}^\top H_n$ in (9) is usually expensive. It is referred to the matricized-tensor times Khatri–Rao product (MTTKRP) [23], which takes $\mathcal{O}(RI_1 I_2 I_3)$ operations. When the value of I_n ($n = 1, \dots, 3$) is large, the cost of computing the gradient (9) is often prohibitively expensive, rendering most traditional deterministic first-order optimization algorithms ineffective. Rank- $(L_r, L_r, 1)$ BTD presents a distinct structural configuration, meriting further exploration in applying the stochastic gradient method.

2.2 Stochastic methods with inertial acceleration for tensor decomposition

If $L_r = 1$, the decomposition format in (4) is CP decomposition and (7) is a CP decomposition type subproblem. The iBrasCPD [45] updates the factor variables by

$$\begin{aligned} A_n^{k+1} &= \arg \min_{A_n} h_n(A_n) + \langle \tilde{\nabla}_{A_n} f(\underline{A}_n^k), A_n - \tilde{A}_n^k \rangle + \frac{1}{2\eta^k} \|A_n - \tilde{A}_n^k\|_F^2, \\ A_{n'}^{k+1} &= A_{n'}^k, \quad n' \neq n, \end{aligned} \quad (10)$$

where $\tilde{\nabla}_{A_n} f(\underline{A}_n^k) = \tilde{\nabla}_{A_n} f(A_1^k \cdots \underline{A}_n^k \cdots A_N^k)$ with inertial acceleration $\underline{A}_n^k = A_n^k + \beta^k(A_n^k - A_n^{k-1})$ and $\tilde{A}_n^k = A_n^k + \alpha^k(A_n^k - A_n^{k-1})$ for proximal term. When $\alpha^k = \beta^k = 0$, then the iBrasCPD algorithm is reduced to BrasCPD [14]; if $\alpha^k = 0$, then the iBrasCPD equals to mBrasCPD [43].

If $h_n(\cdot)$ is a closed proper convex function, (10) can be solved by applying the proximal operator of $h_n(\cdot)$, which is denoted as

$$A_n^{k+1} = \text{Prox}_{\eta^k h_n} \left(\tilde{A}_n^k - \eta^k \tilde{\nabla}_{A_n} f(\underline{A}_n^k) \right). \quad (11)$$

The variance-reduced gradient estimators are also taken into consideration. One of the popular variance-reduced gradient estimators is SAGA [10], which is formulated as follows

$$\tilde{G}_n^k := \frac{1}{I_n |\mathcal{F}_n^k|} \left(\sum_{j \in \mathcal{F}_n^k} \nabla_{A_n} f_j(A^k) - \nabla_{A_n} f_j((\tilde{A}^k)^j) \right) + \frac{1}{J_n} \sum_{i=1}^{J_n} \nabla_{A_n} f_i((\tilde{A}^k)^i), \quad (12)$$

where $A^k := (A_1^k, \dots, A_N^k)$, and the variables $(\tilde{A}^k)^i$ are updated by $(\tilde{A}^k)^i = \tilde{A}^k$ if $i \in \mathcal{F}_n^k$ and $(\tilde{A}^k)^i = (\tilde{A}^{k-1})^i$ otherwise.

The update scheme in (10) employs one-step inertial acceleration, which improves the global convergence of the iterates. However, when the parameters α^k , β^k , and L_r are not carefully chosen, this method may not demonstrate significant acceleration compared to using the SAGA estimator without any acceleration. To better illustrate the effectiveness of the acceleration method, the multi-step inertial scheme was proposed in [27], which can be given by

$$\begin{aligned} \tilde{x}^k &= x^k + \sum_{i=1}^t \alpha^{k+1-i} (x^{k+1-i} - x^{k-i}), \\ \underline{x}^k &= x^k + \sum_{i=1}^t \beta^{k+1-i} (x^{k+1-i} - x^{k-i}), \\ x^{k+1} &= \tilde{x}^k - \eta^k \nabla f(\underline{x}^k). \end{aligned}$$

Figure 3 demonstrates that the multi-step inertial scheme offers greater flexibility and possibly achieves better acceleration than the one-step approach. Multi-step acceleration also allows even a negative inertial parameter, which performs better than all nonnegative parameters, but for one-step acceleration, a negative parameter is not a good choice.

3 Multi-step inertial accelerated doubly SGD algorithm

In this section, we firstly introduce a multi-step inertial accelerated doubly stochastic gradient descent algorithm, a novel approach tailored for the rank- $(L_r, L_r, 1)$ block term decomposition problem (6), denoted by Midas-LL1. This algorithm optimizes all partitioned matrices of every

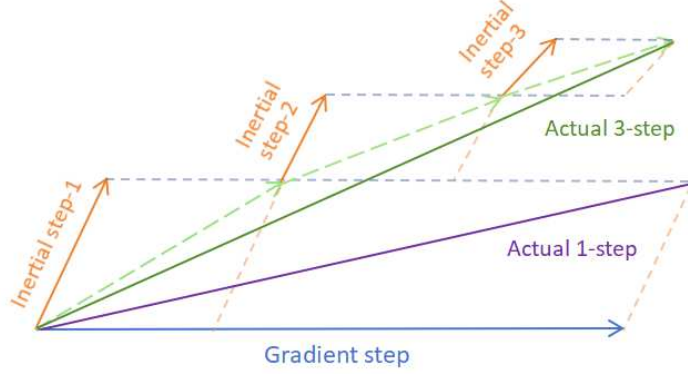


Figure 3: The illustration of multi-step inertial acceleration.

factor in parallel, using a gradient descent mechanism enhanced with a multi-step inertial framework to improve convergence.

We first reformulate the subproblem (7) equivalently as

$$A_{n,r}^* = \arg \min_{A_{n,r}} \frac{1}{2I^3} \left\| X_{(n)} - \sum_{r=1}^R H_{n,r} A_{n,r}^\top \right\|_F^2 + h_n(A_{n,r}), \quad (13)$$

where $\sum_{r=1}^R h_n(A_{n,r}) = h_n(A_n)$. The gradient of f with respect to partition-wise factor $A_{n,r}$ for $r = 1, 2, \dots, R$ is equal to

$$\nabla_{A_{n,r}} f(A_1, A_2, A_3) = \frac{1}{IN} \left(\left(\sum_{r=1}^R H_{n,r} A_{n,r}^\top \right)^\top H_{n,r} - X_{(n)}^\top H_{n,r} \right) = \frac{1}{IN} (A_n H_n^\top H_{n,r} - X_{(n)}^\top H_{n,r}), \quad (14)$$

where $H_{n,r}$ is the partition-wise Kronecker product in (8). Let $\tilde{\nabla}_{A_{n,r}} f \in \mathbb{R}^{I_n \times L_r}$ be the stochastic gradient of $f(A_1, A_2, A_3)$ for $A_{n,r}$, $n = 1, 2, 3$, then we have

$$\tilde{\nabla}_{A_{n,r}} f(A_1, A_2, A_3) = \frac{1}{I_n |\mathcal{F}_n|} (A_n H_n^\top(\mathcal{F}_n) H_{n,r}(\mathcal{F}_n) - X_n^\top(\mathcal{F}_n) H_{n,r}(\mathcal{F}_n)), \quad (15)$$

where

$$X_n(\mathcal{F}_n) = X_n(\mathcal{F}_n, :), \quad H_n(\mathcal{F}_n) = H_n(\mathcal{F}_n, :).$$

At each iteration, we choose one index n from $\{1, \dots, N\}$ in order and randomly sample some fiber indexes \mathcal{F}_n from $\{1, \dots, J_n\}$. Figure 4 shows the fiber-sampling strategy for the stochastic gradient with batch size $|\mathcal{F}_n| = 3$.

We compute the multi-step inertial accelerated stochastic gradient estimator $\tilde{\nabla}_{A_{n,r}} f(\dots, \underline{A}_n^k, \dots)$, shortly denoted as $\tilde{\nabla}_{A_{n,r}} f(\underline{A}_n^k)$. At last, we update A_n^{k+1} by the stochastic proximal gradient descent method.

The algorithmic framework of Midas-LL1 (Algorithm 1) for optimization problem (6) is presented as follows.

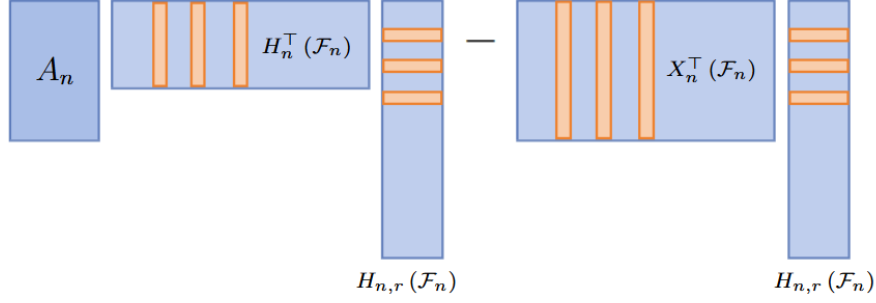


Figure 4: Fiber-sampling strategy with batchsize $|\mathcal{F}_n| = 3$.

Algorithm 1 Midas-LL1: multi-step inertial accelerated doubly SGD for rank- $(L_r, L_r, 1)$ block-term decomposition problem (6)

Input: A third-order tensor $\mathcal{X} \in \mathbb{R}^{I_1 \times I_2 \times I_3}$; the rank of partitioned factors in vector $L = [L_1, \dots, L_R]$; the number of components R ; the sample size B ; initialization $\{A_n^{-1}\}_{n=1}^3 = \{A_n^0\}_{n=1}^3$, setting stepsize $\{\eta^k\}_{k \geq 0}$; an integer $t \geq 1$, and inertial parameters $\{\alpha^{k+1-i}\}_{k \geq 0}, \{\beta^{k+1-i}\}_{k \geq 0} \in [0, 1]$ with $i \in \{1, \dots, t\}$.

- 1: $k \leftarrow 0$;
- 2: **repeat**
- 3: Sample n uniformly from $\{1, \dots, N\}$.
- 4: Sample \mathcal{F}_n uniformly from $\{1, \dots, J_n\}$ with $|\mathcal{F}_n| = B$.
- 5: Set $\tilde{A}_n^k = A_n^k + \sum_{i=1}^t \alpha^{k+1-i} (A_n^{k+1-i} - A_n^{k-i})$, $\underline{A}_n^k = A_n^k + \sum_{i=1}^t \beta^{k+1-i} (A_n^{k+1-i} - A_n^{k-i})$.
- 6: Compute stochastic gradient $\tilde{\nabla}_{A_{n,r}} f(\underline{A}_n^k)$ with the minibatch B that satisfies Definition 3.
- 7: Update partitioned matrices $A_{n,r}^{k+1}$ of A_n^{k+1} for $r = 1, \dots, R$ and A_n^{k+1} :

$$A_{n,r}^{k+1} = \arg \min_{A_{n,r}} h_n(A_{n,r}) + \langle \tilde{\nabla}_{A_{n,r}} f(\underline{A}_n^k), A_{n,r} - (\tilde{A}_{n,r})^k \rangle + \frac{1}{2\eta^k} \|A_{n,r} - (\tilde{A}_{n,r})^k\|_F^2, \quad (16)$$

$$A_{n'}^{k+1} = A_{n'}^k, \quad \forall n' \neq n.$$

- 8: $k \leftarrow k + 1$;
- 9: **until** some stopping criterion is reached;

Output: $\{A_n^k\}_{n=1}^N$.

Remark 1. The Midas-LL1 serves as a general algorithm framework:

- (i) If $L_r = 1$ for $r = 1, \dots, R$, and $t = 1$, then Midas-LL1 (Algorithm 1) is equivalent to iBrasCPD [45].
- (ii) If $L_r = 1$ for $r = 1, \dots, R$, and $t = 0$, then Midas-LL1 algorithm is similar to BrasCPD [14] with vanilla SGD.

Assumption 1. (i) $h_n : \mathbb{R}^{I_n \times R} \rightarrow \mathbb{R} \cup \{+\infty\}$ are proper lower semi-continuous (l.s.c.) functions that are bounded from below, and $h(\cdot)$ is convex.

- (ii) The sequence $\{A_1^k, A_2^k, A_3^k\}$ generated by Algorithm 1 is bounded for all k .

Remark 2. (i) Suppose Assumption 1 (ii) holds, then for any factors $\{A_1, A_2, A_3\}$, $\{\underline{A}_1, \underline{A}_2, \underline{A}_3\}$ and any mode $n \in \{1, 2, 3\}$, there exists a constant L such that

$$\|\nabla_{A_n} f(\dots, \bar{A}_n, \dots) - \nabla_{A_n} f(\dots, A_n, \dots)\|_F \leq L \|\bar{A}_n - A_n\|_F,$$

which shows that

$$|f(\dots, A_n, \dots) - f(\dots, \underline{A}_n, \dots) - \langle \nabla_{A_n} f(\dots, \underline{A}_n, \dots), A_n - \underline{A}_n \rangle| \leq \frac{L}{2} \|A_n - \bar{A}_n\|_F^2. \quad (17)$$

In fact, $f(A_1, A_2, A_3)$ is quadratic with respect to A_n , for all $n \in \{1, 2, 3\}$, and the quadratic term is $\frac{1}{2I^n} A_n^\top (H_n^\top H_n) A_n$. Hence, we have (17) holds with

$$L \geq \frac{1}{I^3} \max\{\lambda_{\max}(H_n^\top H_n)\}$$

for any $n \in \{1, 2, 3\}$.

(ii) The optimal objective value Φ^* of the objective function $\Phi(A_1, A_2, A_3)$ defined by (6) is finite under Assumption 1 (ii).

Let ξ^k and ζ^k be the stochastic parameters for the block index and the stochastic gradient, respectively. Denote $\mathbb{E}_k[\cdot] = \mathbb{E}[\cdot | \xi^k, \zeta^k]$ and $\mathbb{E}[\cdot] = \mathbb{E}[\cdot | \xi^0, \zeta^0, \dots]$.

Definition 3. (Multi-step variance-reduced stochastic gradient) We say a gradient estimator $\tilde{\nabla}_{A_{\xi^k}} f$ with ξ^k randomly selected from the index set $\{1, 2, 3\}$, is variance-reduced with constants $V_1, V_2, V_\Gamma \geq 0$, $t \geq 1$, and $\tau \in (0, 1]$ if it satisfies the following conditions:

(i) (Mean squared error (MSE) bound): there exists a sequence of random variables $\{\Gamma_k\}_{k \geq 1}$ such that

$$\mathbb{E}_k[\|\tilde{\nabla}_{A_{\xi^k}} f(\underline{A}_{\xi^k}^k) - \nabla_{A_{\xi^k}} f(\underline{A}_{\xi^k}^k)\|_F^2] \leq \Gamma_k + V_1 \left(\sum_{i=1}^{t+1} \|A^{k+1-i} - A^{k-i}\|_F^2 \right), \quad (18)$$

and random variables $\{\Upsilon_k\}_{k \geq 1}$ such that

$$\mathbb{E}_k[\|\tilde{\nabla}_{A_{\xi^k}} f(\underline{A}_{\xi^k}^k) - \nabla_{A_{\xi^k}} f(\underline{A}_{\xi^k}^k)\|_F] \leq \Upsilon_k + V_2 \left(\sum_{i=1}^{t+1} \|A^{k+1-i} - A^{k-i}\|_F \right). \quad (19)$$

(ii) (Geometric decay): The sequence $\{\Gamma_k\}_{k \geq 1}$ satisfy the following inequality in expectation:

$$\mathbb{E}_k[\Gamma_{k+1}] \leq (1 - \tau)\Gamma_k + V_\Gamma \left(\sum_{i=1}^{t+1} \|A^{k+1-i} - A^{k-i}\|_F^2 \right). \quad (20)$$

(iii) (Convergence of estimator): For all sequences $\{A^k\}_{k=0}^\infty$, if $\lim_{k \rightarrow \infty} \mathbb{E} \|A^k - A^{k-1}\|_F^2 \rightarrow 0$, then it follows that $\mathbb{E}\Gamma_k \rightarrow 0$ and $\mathbb{E}\Upsilon_k \rightarrow 0$.

4 Convergence analysis

This section is dedicated to the convergence analysis of the sequence generated by Algorithm 1.

4.1 Subsequential convergence analysis

We first present the descent of $\Phi(A_1^{k+1}, A_2^{k+1}, A_3^{k+1})$ under expectation in the following lemma.

Lemma 1. *Suppose $\{A_1^k, A_2^k, A_3^k\}_{k \in \mathbb{N}}$ is the sequence generated by Algorithm 1. Assume that Assumption 1 holds and $\tilde{\nabla}_{A_{n,r}} f$ with $n = 1, 2, 3$ is variance-reduced as defined in Definition 3. Define the following quantities for $k \in \mathbb{N}$,*

$$b_k \stackrel{\text{def}}{=} \frac{1 - \sum_{i=1}^t \alpha^{k+1-i} - 2L\eta^k - \gamma\eta^k}{2\eta^k}, \quad \underline{b} \stackrel{\text{def}}{=} \liminf_{k \in \mathbb{N}} b_k, \quad (21)$$

and

$$a_{k,i} \stackrel{\text{def}}{=} \frac{3Lt(\beta^{k+1-i})^2}{2} + \frac{\gamma}{2} + \frac{\alpha^{k+1-i}}{2\eta^k}, \quad \bar{a}_i \stackrel{\text{def}}{=} \limsup_{k \in \mathbb{N}} a_{k,i}. \quad (22)$$

Here, $\gamma = \sqrt{(V_\Gamma/\tau + V_1)}$, $V_1, V_2, V_\Gamma \geq 0$, $\tau \in (0, 1]$ are parameters in Definition 3, and $\{\alpha^{k+1-i}\}_{k \geq 0}$, $\{\beta^{k+1-i}\}_{k \geq 0} \in [0, 1]$ are inertial parameters in Algorithm 1. Then the following inequality holds for any $k > 0$,

$$\begin{aligned} & \mathbb{E}_k[\Phi(A_1^{k+1}, A_2^{k+1}, A_3^{k+1})] + \underline{b} \mathbb{E}_k \left[\|A^{k+1} - A^k\|_F^2 \right] + \frac{1}{2\gamma\tau} \mathbb{E}_k[\Gamma_{k+1}] \\ & \leq \Phi(A_1^k, A_2^k, A_3^k) + \frac{1}{2\gamma\tau} \Gamma_k + \sum_{i=1}^t \bar{a}_i \|A^{k+1-i} - A^{k-i}\|_F^2 + \frac{\gamma}{2} \|A^{k-t} - A^{k-t-1}\|_F^2. \end{aligned}$$

Proof. Assume $n = \xi^k$ at the k -th iteration. Based on the update rule for $A_{\xi^k, r}^{k+1}$ in Midas-LL1 framework (Algorithm 1), we establish that

$$A_{\xi^k, r}^{k+1} = \arg \min_{A_{\xi^k, r}} h_{\xi^k}(A_{\xi^k, r}) + \langle \tilde{\nabla}_{A_{\xi^k, r}} f(A_{\xi^k}^k), A_{\xi^k, r} - \tilde{A}_{\xi^k, r}^k \rangle + \frac{1}{2\eta^k} \|A_{\xi^k, r} - \tilde{A}_{\xi^k, r}^k\|_F^2.$$

The inequality below holds by definition of $A_{\xi^k, r}^{k+1}$

$$\begin{aligned} & \sum_{r=1}^R \left(h_{\xi^k}(A_{\xi^k, r}^{k+1}) + \langle \tilde{\nabla}_{A_{\xi^k, r}} f(A_{\xi^k}^k), A_{\xi^k, r}^{k+1} - \tilde{A}_{\xi^k, r}^k \rangle + \frac{1}{2\eta^k} \|A_{\xi^k, r}^{k+1} - \tilde{A}_{\xi^k, r}^k\|_F^2 \right) \\ & \leq \sum_{r=1}^R \left(h_{\xi^k}(A_{\xi^k, r}^k) + \langle \tilde{\nabla}_{A_{\xi^k, r}} f(A_{\xi^k}^k), A_{\xi^k, r}^k - \tilde{A}_{\xi^k, r}^k \rangle + \frac{1}{2\eta^k} \|A_{\xi^k, r}^k - \tilde{A}_{\xi^k, r}^k\|_F^2 \right). \end{aligned} \quad (23)$$

According to (17), we derive

$$\begin{aligned} f(A_1^{k+1}, A_2^{k+1}, A_3^{k+1}) & \leq f(\cdots, \underline{A}_{\xi^k}^k, \cdots) \\ & \quad + \sum_{r=1}^R \langle \nabla_{A_{\xi^k, r}} f(\underline{A}_{\xi^k}^k), A_{\xi^k, r}^{k+1} - \underline{A}_{\xi^k, r}^k \rangle + \sum_{r=1}^R \frac{L}{2} \|A_{\xi^k, r}^{k+1} - \underline{A}_{\xi^k, r}^k\|_F^2, \end{aligned}$$

and

$$\begin{aligned} f(A_1^k, A_2^k, A_3^k) & \geq f(\cdots, \underline{A}_{\xi^k}^k, \cdots) \\ & \quad + \sum_{r=1}^R \langle \nabla_{A_{\xi^k, r}} f(\underline{A}_{\xi^k}^k), A_{\xi^k, r}^k - \underline{A}_{\xi^k, r}^k \rangle - \sum_{r=1}^R \frac{L}{2} \|A_{\xi^k, r}^k - \underline{A}_{\xi^k, r}^k\|_F^2. \end{aligned}$$

Combining two inequalities about f , we can get

$$\begin{aligned}
f(A_1^{k+1}, A_2^{k+1}, A_3^{k+1}) &\leq f(A_1^k, A_2^k, A_3^k) + \sum_{r=1}^R \left\langle \nabla_{A_{\xi^k, r}} f(\underline{A}_{\xi^k}), A_{\xi^k, r}^{k+1} - A_{\xi^k, r}^k \right\rangle \\
&\quad + \sum_{r=1}^R \frac{L}{2} \left\| A_{\xi^k, r}^{k+1} - \underline{A}_{\xi^k, r}^k \right\|_F^2 + \sum_{r=1}^R \frac{L}{2} \left\| A_{\xi^k, r}^k - \underline{A}_{\xi^k, r}^k \right\|_F^2.
\end{aligned} \tag{24}$$

By summing inequalities (23) and (24) together, we derive

$$\begin{aligned}
&\Phi(A_1^{k+1}, A_2^{k+1}, A_3^{k+1}) \\
&\leq \Phi(A_1^k, A_2^k, A_3^k) + \sum_{r=1}^R \left\langle \nabla_{A_{\xi^k, r}} f(\underline{A}_{\xi^k}) - \tilde{\nabla}_{A_{\xi^k, r}} f(\underline{A}_{\xi^k}), A_{\xi^k, r}^{k+1} - A_{\xi^k, r}^k \right\rangle \\
&\quad + \sum_{r=1}^R \frac{L}{2} \left\| A_{\xi^k, r}^{k+1} - \underline{A}_{\xi^k, r}^k \right\|_F^2 + \sum_{r=1}^R \frac{L}{2} \left\| A_{\xi^k, r}^k - \underline{A}_{\xi^k, r}^k \right\|_F^2 \\
&\quad + \sum_{r=1}^R \frac{1}{2\eta^k} \left\| A_{\xi^k, r}^k - \tilde{A}_{\xi^k, r}^k \right\|_F^2 - \sum_{r=1}^R \frac{1}{2\eta^k} \left\| A_{\xi^k, r}^{k+1} - \tilde{A}_{\xi^k, r}^k \right\|_F^2 \\
&\leq \Phi(A_1^k, A_2^k, A_3^k) + \frac{1}{2\gamma^k} \left\| \tilde{\nabla}_{A_{\xi^k}} f(\underline{A}_{\xi^k}) - \nabla_{A_{\xi^k}} f(\underline{A}_{\xi^k}) \right\|_F^2 + \frac{\gamma^k}{2} \left\| A_{\xi^k}^{k+1} - A_{\xi^k}^k \right\|_F^2 \\
&\quad + \frac{3L}{2} \left\| \sum_{i=1}^t \beta^{k+1-i} (A_{\xi^k}^{k+1-i} - A_{\xi^k}^{k-i}) \right\|_F^2 + \frac{1}{2\eta^k} \left\| \sum_{i=1}^t \alpha^{k+1-i} (A_{\xi^k}^{k+1-i} - A_{\xi^k}^{k-i}) \right\|_F^2 \\
&\quad + L \left\| A_{\xi^k}^{k+1} - A_{\xi^k}^k \right\|_F^2 - \frac{1}{2\eta^k} \left\| A_{\xi^k}^{k+1} - \tilde{A}_{\xi^k}^k \right\|_F^2 \\
&\leq \Phi(A_1^k, A_2^k, A_3^k) + \frac{1}{2\gamma^k} \left\| \tilde{\nabla}_{A_{\xi^k}} f(\underline{A}_{\xi^k}) - \nabla_{A_{\xi^k}} f(\underline{A}_{\xi^k}) \right\|_F^2 + \frac{\gamma^k + 2L}{2} \left\| A_{\xi^k}^{k+1} - A_{\xi^k}^k \right\|_F^2 \\
&\quad + \frac{3L}{2} \sum_{i=1}^t t (\beta^{k+1-i})^2 \left\| A_{\xi^k}^{k+1-i} - A_{\xi^k}^{k-i} \right\|_F^2 + \frac{1}{2\eta^k} \left\| \sum_{i=1}^t \alpha^{k+1-i} (A_{\xi^k}^{k+1-i} - A_{\xi^k}^{k-i}) \right\|_F^2 \\
&\quad - \frac{1}{2\eta^k} \left\| A_{\xi^k}^{k+1} - \tilde{A}_{\xi^k}^k \right\|_F^2 \\
&\leq \Phi(A_1^k, A_2^k, A_3^k) + \frac{1}{2\gamma^k} \left\| \tilde{\nabla}_{A_{\xi^k}} f(\underline{A}_{\xi^k}) - \nabla_{A_{\xi^k}} f(\underline{A}_{\xi^k}) \right\|_F^2 + \frac{\gamma^k + 2L}{2} \left\| A_{\xi^k}^{k+1} - A_{\xi^k}^k \right\|_F^2 \\
&\quad + \frac{3L}{2} \sum_{i=1}^t t (\beta^{k+1-i})^2 \left\| A_{\xi^k}^{k+1-i} - A_{\xi^k}^{k-i} \right\|_F^2 + \sum_{i=1}^t \frac{\alpha^{k+1-i}}{2\eta^k} \left\| A_{\xi^k}^{k+1-i} - A_{\xi^k}^{k-i} \right\|_F^2 \\
&\quad - \frac{(1 - \sum_{i=1}^t \alpha^{k+1-i})}{2\eta^k} \left\| A_{\xi^k}^{k+1} - A_{\xi^k}^k \right\|_F^2,
\end{aligned} \tag{25}$$

where $\gamma^k > 0$ is any constant, the second inequality is derived from Young's inequality $\langle a, b \rangle \leq \frac{1}{2c} \|a\|^2 + \frac{c}{2} \|b\|^2$ for $a, b \in \mathbb{R}^n, c \in \mathbb{R}_{++}$. The third inequality is obtained from

$$\left\| A_{\xi^k}^k - \underline{A}_{\xi^k}^k \right\|_F^2 = \left\| \sum_{i=1}^t \beta^{k+1-i} (A_{\xi^k}^{k+1-i} - A_{\xi^k}^{k-i}) \right\|_F^2 \leq \sum_{i=1}^t t (\beta^{k+1-i})^2 \left\| A_{\xi^k}^{k+1-i} - A_{\xi^k}^{k-i} \right\|_F^2,$$

and the last inequality is deduced from

$$\begin{aligned}
& \left\| A_{\xi^k}^{k+1} - \tilde{A}_{\xi^k}^k \right\|_F^2 \\
&= \left\| A_{\xi^k}^{k+1} - A_{\xi^k}^k - \sum_{i=1}^t \alpha^{k+1-i} (A_{\xi^k}^{k+1-i} - A_{\xi^k}^{k-i}) \right\|_F^2 \\
&= \left\| A_{\xi^k}^{k+1} - A_{\xi^k}^k \right\|_F^2 - 2 \sum_{i=1}^t \alpha^{k+1-i} \left\langle A_{\xi^k}^{k+1} - A_{\xi^k}^k, A_{\xi^k}^{k+1-i} - A_{\xi^k}^{k-i} \right\rangle + \left\| \sum_{i=1}^t \alpha^{k+1-i} (A_{\xi^k}^{k+1-i} - A_{\xi^k}^{k-i}) \right\|_F^2 \\
&\geq \left(1 - \sum_{i=1}^t \alpha^{k+1-i}\right) \left\| A_{\xi^k}^{k+1} - A_{\xi^k}^k \right\|_F^2 + \left\| \sum_{i=1}^t \alpha^{k+1-i} (A_{\xi^k}^{k+1-i} - A_{\xi^k}^{k-i}) \right\|_F^2 - \sum_{i=1}^t \alpha^{k+1-i} \left\| A_{\xi^k}^{k+1-i} - A_{\xi^k}^{k-i} \right\|_F^2.
\end{aligned}$$

Applying the conditional expectation operator \mathbb{E}_k to the inequality (25) and constraining the mean squared error term by (18) as specified in Definition 3, we obtain

$$\begin{aligned}
& \mathbb{E}_k[\Phi(A_1^{k+1}, A_2^{k+1}, A_3^{k+1})] \\
&\leq \Phi(A_1^k, A_2^k, A_3^k) + \frac{1}{2\gamma^k} \mathbb{E}_k[\|\tilde{\nabla}_{A_{\xi^k}} f(A_{\xi^k}^k) - \nabla_{A_{\xi^k}} f(A_{\xi^k}^k)\|_F^2] + \frac{\gamma^k + 2L}{2} \mathbb{E}_k[\|A^{k+1} - A^k\|_F^2] \\
&\quad + \frac{3L}{2} \sum_{i=1}^t t (\beta^{k+1-i})^2 \|A^{k+1-i} - A^{k-i}\|_F^2 + \sum_{i=1}^t \frac{\alpha^{k+1-i}}{2\eta^k} \|A^{k+1-i} - A^{k-i}\|_F^2 \\
&\quad - \frac{(1 - \sum_{i=1}^t \alpha^{k+1-i})}{2\eta^k} \mathbb{E}_k[\|A^{k+1} - A^k\|_F^2] \\
&\leq \Phi(A_1^k, A_2^k, A_3^k) + \frac{1}{2\gamma^k \tau} (\Gamma_k - \mathbb{E}_k[\Gamma_{k+1}]) + \left(\frac{\gamma^k + 2L}{2} - \frac{(1 - \sum_{i=1}^t \alpha^{k+1-i})}{2\eta^k} \right) \mathbb{E}_k[\|A^{k+1} - A^k\|_F^2] \\
&\quad + \left(\frac{V_\Gamma}{2\gamma^k \tau} + \frac{V_1}{2\gamma^k} \right) \left(\sum_{i=1}^{t+1} \|A^{k+1-i} - A^{k-i}\|_F^2 \right) + \frac{3L}{2} \sum_{i=1}^t t (\beta^{k+1-i})^2 \|A^{k+1-i} - A^{k-i}\|_F^2 \\
&\quad + \sum_{i=1}^t \frac{\alpha^{k+1-i}}{2\eta^k} \|A^{k+1-i} - A^{k-i}\|_F^2.
\end{aligned} \tag{26}$$

Let $\gamma = \gamma^k = \sqrt{(V_\Gamma/\tau + V_1)}$, then we can get

$$\begin{aligned}
& \mathbb{E}_k[\Phi(A_1^{k+1}, A_2^{k+1}, A_3^{k+1})] + \left(\frac{(1 - \sum_{i=1}^t \alpha^{k+1-i})}{2\eta^k} - \frac{\gamma + 2L}{2} \right) \mathbb{E}_k[\|A^{k+1} - A^k\|_F^2] + \frac{1}{2\gamma\tau} \mathbb{E}_k[\Gamma_{k+1}] \\
&\leq \Phi(A_1^k, A_2^k, A_3^k) + \frac{1}{2\gamma\tau} \Gamma_k + \sum_{i=1}^t \left(\frac{3Lt (\beta^{k+1-i})^2}{2} + \frac{\gamma}{2} + \frac{\alpha^{k+1-i}}{2\eta^k} \right) \|A^{k+1-i} - A^{k-i}\|_F^2 \\
&\quad + \frac{\gamma}{2} \|A^{k-t} - A^{k-t-1}\|_F^2.
\end{aligned}$$

Denote b_k and $a_{k,i}$ as in (21) and (22), respectively. Consequently, we obtain

$$\begin{aligned}
& \mathbb{E}_k[\Phi(A_1^{k+1}, A_2^{k+1}, A_3^{k+1})] + \underline{b} \mathbb{E}_k[\|A^{k+1} - A^k\|_F^2] + \frac{1}{2\gamma\tau} \mathbb{E}_k[\Gamma_{k+1}] \\
& \leq \mathbb{E}_k[\Phi(A_1^{k+1}, A_2^{k+1}, A_3^{k+1})] + b_k \mathbb{E}_k[\|A^{k+1} - A^k\|_F^2] + \frac{1}{2\gamma\tau} \mathbb{E}_k[\Gamma_{k+1}] \\
& \leq \Phi(A_1^k, A_2^k, A_3^k) + \frac{1}{2\gamma\tau} \Gamma_k + \sum_{i=1}^t a_{k,i} \|A^{k+1-i} - A^{k-i}\|_F^2 + \frac{\gamma}{2} \|A^{k-t} - A^{k-t-1}\|_F^2 \\
& \leq \Phi(A_1^k, A_2^k, A_3^k) + \frac{1}{2\gamma\tau} \Gamma_k + \sum_{i=1}^t \bar{a}_i \|A^{k+1-i} - A^{k-i}\|_F^2 + \frac{\gamma}{2} \|A^{k-t} - A^{k-t-1}\|_F^2.
\end{aligned}$$

Hence, the proof is completed. \square

Following this, a new Lyapunov function is introduced. We prove that it is monotonically nonincreasing in expectation. To simplify notation, we denote $\Phi^k = \Phi(A_1^k, A_2^k, A_3^k)$.

Lemma 2. *Assume that Assumption 1 holds and $\tilde{\nabla}_{A_{n,r}} f$ for $n = 1, 2, 3$ is variance-reduced as defined in Definition 3. Let $\{A_1^k, A_2^k, A_3^k\}_{k \in \mathbb{N}}$ be a sequence generated by Algorithm 1. We then define the following Lyapunov sequence*

$$\Psi_k := \Phi^k + \sum_{i=1}^{t+1} \sum_{j=i}^{t+1} (j+1) \bar{a}_j \|A^{k+1-i} - A^{k-i}\|_F^2 + \frac{1}{2\tau\gamma} \Gamma_k, \quad (27)$$

and choose η^k , γ , $\{\alpha^{k+1-i}\}_{k \geq 0}$, and $\{\beta^{k+1-i}\}_{k \geq 0}$ in (21) and (22) such that

$$\delta = \underline{b} - \sum_{j=1}^{t+1} (j+1) \bar{a}_j > 0, \quad \text{and} \quad (t+2) \bar{a}_{t+1} - \frac{\gamma}{2} > 0. \quad (28)$$

Then, for all $k \in \mathbb{N}$, we have

$$\mathbb{E}_k[\Psi_{k+1}] \leq \Psi_k - \rho \left(\mathbb{E}_k[\|A^{k+1} - A^k\|_F^2] + \sum_{i=1}^{t+1} \|A^{k+1-i} - A^{k-i}\|_F^2 \right), \quad (29)$$

where $\rho := \min\{\delta, (t+2) \bar{a}_{t+1} - \frac{\gamma}{2}, \bar{a}\}$.

Proof. According to Lemma 1, we have

$$\begin{aligned}
& \mathbb{E}_k[\Phi^{k+1}] - \Phi^k \\
& \leq \sum_{i=1}^t \bar{a}_i \|A^{k+1-i} - A^{k-i}\|_F^2 + \frac{\gamma}{2} \|A^{k-t} - A^{k-t-1}\|_F^2 - \underline{b} \mathbb{E}_k[\|A^{k+1} - A^k\|_F^2] \\
& \quad - \frac{1}{2\gamma\tau} (\mathbb{E}_k[\Gamma_{k+1}] - \Gamma_k).
\end{aligned} \quad (30)$$

Furthermore, by using (27) and integrating it with (30), we obtain

$$\begin{aligned}
& \Psi_k - \mathbb{E}_k[\Psi_{k+1}] \\
& = \sum_{i=1}^{t+1} \sum_{j=i}^{t+1} (j+1) \bar{a}_j \|A^{k+1-i} - A^{k-i}\|_F^2 - \sum_{i=1}^{t+1} \sum_{j=i}^{t+1} (j+1) \bar{a}_j \mathbb{E}_k[\|A^{k+2-i} - A^{k+1-i}\|_F^2] + \Phi^k - \mathbb{E}_k[\Phi_{k+1}]
\end{aligned}$$

$$\begin{aligned}
& + \frac{1}{2\tau\gamma}(\Gamma_k - \mathbb{E}_k[\Gamma_{k+1}]) \\
\geq & \underline{b} \mathbb{E}_k[\|A^{k+1} - A^k\|_F^2] - \sum_{i=1}^t \bar{a}_i \|A^{k+1-i} - A^{k-i}\|_F^2 + \left((t+2)\bar{a}_{t+1} - \frac{\gamma}{2}\right) \|A^{k-t} - A^{k-t-1}\|_F^2 \\
& + \sum_{i=1}^t \sum_{j=i}^{t+1} (j+1)\bar{a}_j \|A^{k+1-i} - A^{k-i}\|_F^2 - \sum_{j=1}^{t+1} (j+1)\bar{a}_j \mathbb{E}_k[\|A^{k+1} - A^k\|_F^2] \\
& - \sum_{i=2}^{t+1} \sum_{j=i}^{t+1} (j+1)\bar{a}_j \|A^{k+2-i} - A^{k+1-i}\|_F^2 \\
\geq & (\underline{b} - \sum_{j=1}^{t+1} (j+1)\bar{a}_j) \mathbb{E}_k[\|A^{k+1} - A^k\|_F^2] + \left((t+2)\bar{a}_{t+1} - \frac{\gamma}{2}\right) \|A^{k-t} - A^{k-t-1}\|_F^2 \\
& + \sum_{i=1}^t \sum_{j=i}^{t+1} \bar{a}_j \|A^{k+1-i} - A^{k-i}\|_F^2 - \sum_{i=1}^t \bar{a}_i \|A^{k+1-i} - A^{k-i}\|_F^2 - \sum_{i=2}^{t+1} \sum_{j=i}^{t+1} \bar{a}_j \|A^{k+2-i} - A^{k+1-i}\|_F^2 \\
& + \sum_{i=1}^t \sum_{j=i}^{t+1} j\bar{a}_j \|A^{k+1-i} - A^{k-i}\|_F^2 - \sum_{i=2}^{t+1} \sum_{j=i}^{t+1} j\bar{a}_j \|A^{k+2-i} - A^{k+1-i}\|_F^2 \\
\geq & (\underline{b} - \sum_{j=1}^{t+1} (j+1)\bar{a}_j) \mathbb{E}_k[\|A^{k+1} - A^k\|_F^2] + \left((t+2)\bar{a}_{t+1} - \frac{\gamma}{2}\right) \|A^{k-t} - A^{k-t-1}\|_F^2 \\
& + \sum_{i=1}^t i\bar{a}_i \|A^{k+1-i} - A^{k-i}\|_F^2 \\
\geq & \delta \mathbb{E}_k[\|A^{k+1} - A^k\|_F^2] + \left((t+2)\bar{a}_{t+1} - \frac{\gamma}{2}\right) \|A^{k-t} - A^{k-t-1}\|_F^2 + \bar{a} \sum_{i=1}^t \|A^{k+1-i} - A^{k-i}\|_F^2,
\end{aligned}$$

where the last inequality follows from (28), and $\bar{a} = \min_{i \in \{1, \dots, t\}} \bar{a}_i$. The third inequality stems from the fact that

$$\begin{aligned}
& \sum_{i=1}^t \bar{a}_i \|A^{k+1-i} - A^{k-i}\|_F^2 + \sum_{i=2}^{t+1} \sum_{j=i}^{t+1} \bar{a}_j \|A^{k+2-i} - A^{k+1-i}\|_F^2 \\
= & \sum_{i=1}^t \bar{a}_i \|A^{k+1-i} - A^{k-i}\|_F^2 + \sum_{i=1}^t \sum_{j=i+1}^{t+1} \bar{a}_j \|A^{k+1-i} - A^{k-i}\|_F^2 = \sum_{i=1}^t \sum_{j=i}^{t+1} \bar{a}_j \|A^{k+1-i} - A^{k-i}\|_F^2,
\end{aligned}$$

and

$$\begin{aligned}
& \sum_{i=1}^t \sum_{j=i}^{t+1} j\bar{a}_j \|A^{k+1-i} - A^{k-i}\|_F^2 - \sum_{i=2}^{t+1} \sum_{j=i}^{t+1} j\bar{a}_j \|A^{k+2-i} - A^{k+1-i}\|_F^2 \\
= & \sum_{i=1}^t \sum_{j=i}^{t+1} j\bar{a}_j \|A^{k+1-i} - A^{k-i}\|_F^2 - \sum_{i=1}^t \sum_{j=i+1}^{t+1} j\bar{a}_j \|A^{k+1-i} - A^{k-i}\|_F^2 = \sum_{i=1}^t i\bar{a}_i \|A^{k+1-i} - A^{k-i}\|_F^2.
\end{aligned}$$

Denote $\rho := \min\{\delta, (t+2)\bar{a}_{t+1} - \frac{\gamma}{2}, \bar{a}\}$. Then we have

$$\Psi_k - \mathbb{E}_k[\Psi_{k+1}] \geq \rho (\mathbb{E}_k[\|A^{k+1} - A^k\|_F^2] + \sum_{i=1}^t \|A^{k+1-i} - A^{k-i}\|_F^2 + \|A^{k-t} - A^{k-t-1}\|_F^2).$$

Therefore, the proof is completed. \square

Remark 3. Given that η^k lies in $[\underline{\eta}, \bar{\eta}]$. From (21), (22), and (28), the following can be concluded:

- (i) When $\alpha^{k+1-i} = \beta^{k+1-i} \equiv 0$ in (21) and (22), condition (28) holds as long as $\bar{\eta} < \frac{2}{4L + \gamma(t+2)(t+3)}$.
- (ii) Set $t = 1$. If $\alpha^k \equiv \alpha$, $\beta^k \equiv \beta$ (i.e. constant inertial parameters), then (28) implies that α , β must lie within a certain region defined by the inequality,

$$L\beta^2 < \frac{1 - 2L\bar{\eta} - 6\gamma\bar{\eta} - 6\alpha}{15\bar{\eta}}.$$

- (iii) When $t \geq 2$, for each $i \in \{1, \dots, t\}$, let $\alpha^{k+1-i} \equiv \alpha^i$, $\beta^{k+1-i} \equiv \beta^i$, then (28) tells us that the β^i must live in a region related to α^i ,

$$\frac{3Lt}{2} \sum_{i=1}^{t+1} (i+1)(\beta^i)^2 < \frac{1 - \sum_{j=1}^t (i+2)\alpha^i - (t+2)\alpha^{t+1} - 2L\bar{\eta}}{2\bar{\eta}} - \frac{\gamma(t+2)(t+3)}{4}.$$

As indicated by Lemma 2, Ψ_{k+1} becomes nonincreasing in expectation if the stepsize η^k , the inertial parameters $\{\alpha^{k+1-i}\}_{k \geq 0}$, and $\{\beta^{k+1-i}\}_{k \geq 0}$ are appropriately selected. Based on this result, we demonstrate our main conclusion in this subsection.

Theorem 1. Given the sequence $\{A_1^k, A_2^k, A_3^k\}_{k \in \mathbb{N}}$ generated by the Algorithm 1, the following conclusions can be drawn.

- (i) The sequence $\{\mathbb{E}[\Psi_k]\}_{k \in \mathbb{N}}$ is monotonically nonincreasing.
- (ii) $\sum_{k=1}^{+\infty} \mathbb{E}[\|A^{k+1} - A^k\|_F^2] < +\infty$, indicating that $\mathbb{E}[\|A^{k+1} - A^k\|_F^2] \rightarrow 0$ as $k \rightarrow \infty$.
- (iii) For any positive integer K , we have $\min_{1 \leq k \leq K} \mathbb{E}[\|A^{k+1} - A^k\|_F^2] \leq \frac{\Psi_1}{\epsilon K}$.

Proof. (i) This statement follows directly from Lemma 2, which ensures the nonincreasing nature of the sequence $\{\mathbb{E}[\Psi_k]\}_{k \in \mathbb{N}}$ since $\epsilon > 0$.

- (ii) Accumulating (29) from $k = 1$ to a positive integer K , we obtain

$$\sum_{k=1}^K \mathbb{E}[\|A^{k+1} - A^k\|_F^2] \leq \frac{1}{\epsilon} \mathbb{E}[\Psi_1 - \Psi_{K+1}] \leq \frac{1}{\epsilon} \Psi_1,$$

where the last inequality follows from the non-negativity of Ψ_k for any $k > 0$. Taking the limit as $K \rightarrow +\infty$, we have

$$\sum_{k=1}^{+\infty} \mathbb{E}[\|A^{k+1} - A^k\|_F^2] < +\infty.$$

Therefore, it follows that the sequence $\{\mathbb{E}[\|A^{k+1} - A^k\|_F^2]\}$ converges to zero.

- (iii) For any positive integer K , the following inequality is satisfied

$$K \min_{1 \leq k \leq K} \mathbb{E}[\|A^{k+1} - A^k\|_F^2] \leq \sum_{k=1}^K \mathbb{E}[\|A^{k+1} - A^k\|_F^2] \leq \frac{1}{\epsilon} \Psi_1,$$

which yields the desired result.

This completes the proof. \square

4.2 Sequential convergence analysis

In this subsection, we explore the sequential convergence of the Midas-LL1 algorithm, demonstrating the convergence of the entire sequence to an ϵ -stationary point.

Lemma 3. *Suppose that Assumption 1 holds, the stepsize η^k lies in $[\underline{\eta}, \bar{\eta}]$, (28) is satisfied, and assume that the sequences $\{\alpha^{k+1-i}\}_{i=1}^t$ and $\{\beta^{k+1-i}\}_{i=1}^t$ are both non-decreasing with limits $\lim_{k \rightarrow \infty} \alpha_k = c_1$ and $\lim_{k \rightarrow \infty} \beta_k = c_2$. Let $\{A_1^k, A_2^k, A_3^k\}_{k \in \mathbb{N}}$ be a bounded sequence generated by Algorithm 1. Define*

$$P_{\xi^k}^{k+1} := \nabla_{A_{\xi^k}} f(A^{k+1}) - \tilde{\nabla}_{A_{\xi^k}} f(\underline{A}^k) + \frac{1}{\eta^k} (\tilde{A}_{\xi^k}^k - A_{\xi^k}^{k+1}),$$

where $\underline{A}^k := (\dots, \underline{A}_n^k, \dots)$. Then we have $P_{\xi^k}^{k+1} \in \partial_{\xi^k} \Phi(A^{k+1})$. Furthermore, denote $P^{k+1} = (P_1^{k+1}, P_2^{k+1}, P_3^{k+1})$, where $P_i^{k+1} = P_{\xi^k}^{k+1}$ if $i = \xi^k$ and $P_i^{k+1} = 0$ otherwise. Then $\exists \mathbb{E}_k[P^{k+1}] \in \partial \Phi(A^{k+1})$, and we can obtain the following results

$$\mathbb{E}_k \|P^{k+1}\|_F \leq \mu \left(\mathbb{E}_k \|A^{k+1} - A^k\|_F + \sum_{i=1}^{t+1} \|A^{k+1-i} - A^{k-i}\|_F \right) + \Upsilon_k,$$

where $\mu := \max \left\{ L + \frac{1}{\underline{\eta}}, Lc_2 + \frac{1}{\underline{\eta}}c_1 + V_2, V_2 \right\}$.

Proof. Let $n = \xi^k$ at the k -th iteration. It follows from (16) that

$$\begin{aligned} A_n^{k+1} &= \arg \min_{A_{n,r}} \sum_{r=1}^R h_n(A_{n,r}) + \sum_{r=1}^R \langle \tilde{\nabla}_{A_{n,r}} f(\underline{A}_n^k), A_{n,r} - (\tilde{A}_{n,r})^k \rangle + \frac{1}{2\eta^k} \sum_{r=1}^R \|A_{n,r} - (\tilde{A}_{n,r})^k\|_F^2 \\ &= \arg \min_{A_{n,r}} h_n(A_n) + \langle \tilde{\nabla}_{A_n} f(\underline{A}_n^k), A_n - \tilde{A}_n^k \rangle + \frac{1}{2\eta^k} \|A_n - \tilde{A}_n^k\|_F^2. \end{aligned} \quad (31)$$

Therefore, we derive that

$$0 \in \partial h_n(A_n^{k+1}) + \tilde{\nabla}_{A_n} f(\underline{A}_n^k) + \frac{1}{\eta^k} (A_n^{k+1} - \tilde{A}_n^k).$$

Combining this with

$$\partial_n \Phi(A^{k+1}) = \nabla_{A_n} f(A^{k+1}) + \partial h_n(A_n^{k+1}),$$

we can assert that $P_n^{k+1} \in \partial_n \Phi(A^{k+1})$.

The next step is to derive a bound for the expected value of the norm of P^{k+1} . Let $n = \xi^k$ denote the index selected at the k -th iteration, which suggests that

$$\begin{aligned} & \mathbb{E}_k \|P^{k+1}\|_F \\ &= \mathbb{E}_k \|P_{\xi^k}^{k+1}\|_F \\ &= \mathbb{E}_k \left\| \nabla_{A_{\xi^k}} f(A^{k+1}) - \tilde{\nabla}_{A_{\xi^k}} f(\underline{A}^k) + \frac{1}{\eta^k} (\tilde{A}_{\xi^k}^k - A_{\xi^k}^{k+1}) \right\|_F \\ &\leq \mathbb{E}_k \left\| \nabla_{A_{\xi^k}} f(A^{k+1}) - \tilde{\nabla}_{A_{\xi^k}} f(\underline{A}^k) \right\|_F + \frac{1}{\eta^k} \mathbb{E}_k \|\tilde{A}_{\xi^k}^k - A_{\xi^k}^{k+1}\|_F \\ &\leq \mathbb{E}_k \left\| \nabla_{A_{\xi^k}} f(A^{k+1}) - \nabla_{A_{\xi^k}} f(\underline{A}^k) \right\|_F + \mathbb{E}_k \left\| \nabla_{A_{\xi^k}} f(\underline{A}^k) - \tilde{\nabla}_{A_{\xi^k}} f(\underline{A}^k) \right\|_F + \frac{1}{\eta^k} \mathbb{E}_k \|\tilde{A}_{\xi^k}^k - A_{\xi^k}^{k+1}\|_F \\ &\leq L \mathbb{E}_k \|A^{k+1} - \underline{A}^k\|_F + \Upsilon_k + V_2 \left(\sum_{i=1}^{t+1} \|A^{k+1-i} - A^{k-i}\|_F \right) + \frac{1}{\eta^k} \mathbb{E}_k \|\tilde{A}^k - A^{k+1}\|_F \end{aligned}$$

$$\begin{aligned}
&\leq L\mathbb{E}_k\|A^{k+1} - A^k\|_F + L\left\|\sum_{i=1}^t \beta^{k+1-i}(A^{k+1-i} - A^{k-i})\right\|_F + \Upsilon_k + V_2\sum_{i=1}^t\|A^{k+1-i} - A^{k-i}\|_F \\
&\quad + V_2\|A^{k-t} - A^{k-t-1}\|_F + \frac{1}{\eta^k}\mathbb{E}_k\|A^{k+1} - A^k\|_F + \frac{1}{\eta^k}\left\|\sum_{i=1}^t \alpha^{k+1-i}(A^{k+1-i} - A^{k-i})\right\|_F \\
&\leq \left(L + \frac{1}{\eta^k}\right)\mathbb{E}_k\|A^{k+1} - A^k\|_F + \sum_{i=1}^t \left(L\beta^{k+1-i} + \frac{1}{\eta^k}\alpha^{k+1-i} + V_2\right)\|A^{k+1-i} - A^{k-i}\|_F \\
&\quad + V_2\|A^{k-t} - A^{k-t-1}\|_F + \Upsilon_k \\
&\leq \left(L + \frac{1}{\eta}\right)\mathbb{E}_k\|A^{k+1} - A^k\|_F + \left(L\beta^k + \frac{1}{\eta}\alpha^k + V_2\right)\sum_{i=1}^t\|A^{k+1-i} - A^{k-i}\|_F \\
&\quad + V_2\|A^{k-t} - A^{k-t-1}\|_F + \Upsilon_k \\
&\leq \left(L + \frac{1}{\eta}\right)\mathbb{E}_k\|A^{k+1} - A^k\|_F + \left(Lc_2 + \frac{1}{\eta}c_1 + V_2\right)\sum_{i=1}^t\|A^{k+1-i} - A^{k-i}\|_F \\
&\quad + V_2\|A^{k-t} - A^{k-t-1}\|_F + \Upsilon_k,
\end{aligned}$$

where the last inequality is derived from the sequences $\{\alpha^{k+1-i}\}_{i=1}^t$ and $\{\beta^{k+1-i}\}_{i=1}^t$ are both non-decreasing, i.e., $\alpha^k \geq \alpha^{k-1}$ and $\beta^k \geq \beta^{k-1}$, with limits $\lim_{k \rightarrow \infty} \alpha_k = c_1$ and $\lim_{k \rightarrow \infty} \beta_k = c_2$.

Let $\mu := \max\left\{L + \frac{1}{\eta}, Lc_2 + \frac{1}{\eta}c_1 + V_2, V_2\right\}$, we have

$$\mathbb{E}_k\|P^{k+1}\|_F \leq \mu(\mathbb{E}_k\|A^{k+1} - A^k\|_F + \sum_{i=1}^t\|A^{k+1-i} - A^{k-i}\|_F + \|A^{k-t} - A^{k-t-1}\|_F) + \Upsilon_k,$$

This proves the statement. \square

Lemma 4. *Under the same conditions outlined in Lemma 3, there exists a positive constant $\bar{\mu} := 3 \max\left\{6L^2 + \frac{6}{\eta}, 6L^2t c_2^2 + 3V_1 + \frac{6t}{\eta}c_1^2, 3V_1\right\}$ such that*

$$\mathbb{E}[\text{dist}(0, \partial\Phi(A^{k+1}))^2] \leq \bar{\mu} \left(\mathbb{E}[\|A^{k+1} - A^k\|_F^2] + \sum_{i=1}^{t+1} \|A^{k+1-i} - A^{k-i}\|_F^2 \right) + 3\mathbb{E}\Upsilon_k.$$

Proof. It follows from Lemma 3 that

$$\begin{aligned}
&\mathbb{E}_k\|P^{k+1}\|_F^2 \\
&= \mathbb{E}_k\|P_{\xi^k}^{k+1}\|_F^2 \\
&= \mathbb{E}_k\|\nabla_{A_{\xi^k}} f(A^{k+1}) - \nabla_{A_{\xi^k}} f(\underline{A}^k) + \nabla_{A_{\xi^k}} f(\underline{A}^k) - \tilde{\nabla}_{A_{\xi^k}} f(\underline{A}^k) + \frac{1}{\eta^k}(\tilde{A}_{\xi^k}^k - A_{\xi^k}^{k+1})\|_F^2 \\
&\leq 3\mathbb{E}_k\|\nabla_{A_{\xi^k}} f(A^{k+1}) - \nabla_{A_{\xi^k}} f(\underline{A}^k)\|_F^2 + 3\mathbb{E}_k\|\nabla_{A_{\xi^k}} f(\underline{A}^k) - \tilde{\nabla}_{A_{\xi^k}} f(\underline{A}^k)\|_F^2 + \frac{3}{\eta^k}\mathbb{E}_k\|\tilde{A}^k - A^{k+1}\|_F^2 \\
&\leq 3L^2\mathbb{E}_k\|A^{k+1} - \underline{A}^k\|_F^2 + 3\Gamma_k + 3V_1\sum_{i=1}^{t+1}\|A^{k+1-i} - A^{k-i}\|_F^2 + \frac{3}{\eta^k}\mathbb{E}_k\|A^{k+1} - \tilde{A}^k\|_F^2 \\
&\leq 6L^2\mathbb{E}_k\|A^{k+1} - A^k\|_F^2 + 6L^2t\sum_{i=1}^t(\beta^{k+1-i})^2\|A^{k+1-i} - A^{k-i}\|_F^2 + 3\Gamma_k \\
&\quad + 3V_1\sum_{i=1}^{t+1}\|A^{k+1-i} - A^{k-i}\|_F^2 + \frac{6}{\eta^k}\mathbb{E}_k\|A^{k+1} - A^k\|_F^2 + \frac{6t}{\eta^k}\sum_{i=1}^t(\alpha^{k+1-i})^2\|A^{k+1-i} - A^{k-i}\|_F^2
\end{aligned}$$

$$\begin{aligned}
&\leq (6L^2 + \frac{6}{\underline{\eta}}) \mathbb{E}_k \|A^{k+1} - A^k\|_F^2 + \left(6L^2 t (\beta^k)^2 + 3V_1 + \frac{6t}{\underline{\eta}} (\alpha^k)^2\right) \sum_{i=1}^t \|A^{k+1-i} - A^{k-i}\|_F^2 \\
&\quad + 3V_1 \|A^{k-t} - A^{k-t-1}\|_F^2 + 3\Gamma_k \\
&\leq (6L^2 + \frac{6}{\underline{\eta}}) \mathbb{E}_k \|A^{k+1} - A^k\|_F^2 + \left(6L^2 t c_2^2 + 3V_1 + \frac{6t}{\underline{\eta}} c_1^2\right) \sum_{i=1}^t \|A^{k+1-i} - A^{k-i}\|_F^2 \\
&\quad + 3V_1 \|A^{k-t} - A^{k-t-1}\|_F^2 + 3\Gamma_k \\
&\leq \bar{\mu} (\mathbb{E}_k \|A^{k+1} - A^k\|_F^2 + \sum_{i=1}^t \|A^{k+1-i} - A^{k-i}\|_F^2 + \|A^{k-t} - A^{k-t-1}\|_F^2) + 3\Gamma_k,
\end{aligned}$$

where $\bar{\mu}^0 := \max \left\{ 6L^2 + \frac{6}{\underline{\eta}}, 6L^2 t c_2^2 + 3V_1 + \frac{6t}{\underline{\eta}} c_1^2, 3V_1 \right\}$.

Utilizing $\mathbb{E}_k \left[\text{dist}(0, \partial\Phi(A^{k+1}))^2 \right] \leq 3\mathbb{E}_k \left[\|P^{k+1}\|_F^2 \right]$ and taking the full expectation on both sides, we derive the following result

$$\begin{aligned}
&\mathbb{E}[\text{dist}(0, \partial\Phi(A^{k+1}))^2] \\
&\leq \bar{\mu} \left(\mathbb{E} \|A^{k+1} - A^k\|_F^2 + \sum_{i=1}^t \|A^{k+1-i} - A^{k-i}\|_F^2 + \|A^{k-t} - A^{k-t-1}\|_F^2 \right) + 3\mathbb{E}\Gamma_k,
\end{aligned}$$

where $\bar{\mu} = 3\bar{\mu}^0$. Hence, the proof is finalized. \square

Theorem 2. Suppose Assumptions 1 holds, the stepsize η^k lies in $[\underline{\eta}, \bar{\eta}]$ and (28) is satisfied. Let $\{A_1^k, A_2^k, A_3^k\}_{k \in \mathbb{N}}$ produced by Algorithm 1 remain bounded for all k . Then there exists $0 < \sigma < \epsilon$ such that

$$\mathbb{E}[\text{dist}(0, \partial\Phi(A^{\hat{k}}))^2] \leq \frac{\bar{\mu}}{(\epsilon - \sigma)K} \left(\mathbb{E}\Psi_1 + \frac{3(\epsilon - \sigma)}{\tau\bar{\mu}} \mathbb{E}\Gamma_1 \right) = \mathcal{O}(1/K),$$

where \hat{k} is drawn from $\{2, \dots, K+1\}$. This implies that at most $\mathcal{O}(\epsilon^{-2})$ iterations are required in expectation to reach an ϵ -stationary point (refer to Definition 2) of Φ .

Proof. Combining (29) and Lemma 4, it shows that

$$\begin{aligned}
&\mathbb{E}[\Psi_k - \Psi_{k+1}] \\
&\geq \epsilon (\mathbb{E} \|A^{k+1} - A^k\|_F^2 + \sum_{i=1}^{t+1} \mathbb{E} \|A^{k+1-i} - A^{k-i}\|_F^2) \\
&\geq \sigma (\mathbb{E} \|A^{k+1} - A^k\|_F^2 + \sum_{i=1}^{t+1} \mathbb{E} \|A^{k+1-i} - A^{k-i}\|_F^2) + \frac{\epsilon - \sigma}{\bar{\mu}} \mathbb{E}[\text{dist}(0, \partial\Phi(A^{k+1}))^2] - \frac{3(\epsilon - \sigma)}{\bar{\mu}} \mathbb{E}\Gamma_k \\
&\geq \sigma (\mathbb{E} \|A^{k+1} - A^k\|_F^2 + \sum_{i=1}^{t+1} \mathbb{E} \|A^{k+1-i} - A^{k-i}\|_F^2) + \frac{\epsilon - \sigma}{\bar{\mu}} \mathbb{E}[\text{dist}(0, \partial\Phi(A^{k+1}))^2] \\
&\quad + \frac{3(\epsilon - \sigma)}{\tau\bar{\mu}} \mathbb{E}[\Gamma_{k+1} - \Gamma_k] - \frac{3(\epsilon - \sigma)V_\Gamma}{\tau\bar{\mu}} \sum_{i=1}^{t+1} \mathbb{E} \|A^{k+1-i} - A^{k-i}\|_F^2 \\
&\geq \sigma (\mathbb{E} \|A^{k+1} - A^k\|_F^2 + \sum_{i=1}^{t+1} \mathbb{E} \|A^{k+1-i} - A^{k-i}\|_F^2) + \frac{\epsilon - \sigma}{\bar{\mu}} \mathbb{E}[\text{dist}(0, \partial\Phi(A^{k+1}))^2]
\end{aligned}$$

$$+ \frac{3(\epsilon - \sigma)}{\tau\bar{\mu}} \mathbb{E}[\Gamma_{k+1} - \Gamma_k] - \frac{3(\epsilon - \sigma)V_\Gamma}{\tau\bar{\mu}} \sum_{i=1}^{t+1} \mathbb{E}\|A^{k+1-i} - A^{k-i}\|_F^2 - \frac{3(\epsilon - \sigma)V_\Gamma}{\tau\bar{\mu}} \mathbb{E}\|A^{k+1} - A^k\|_F^2,$$

where the third inequality is derived from (20) in Definition 3. Let $\sigma = \frac{3(\epsilon - \sigma)V_\Gamma}{\tau\bar{\mu}}$, i.e., $\sigma = \frac{3\epsilon V_\Gamma}{\tau\bar{\mu} + 3V_\Gamma}$, it shows that

$$\mathbb{E}[\Psi_k - \Psi_{k+1}] \geq \frac{\epsilon - \sigma}{\bar{\mu}} \mathbb{E}[\text{dist}(0, \partial\Phi(A^{k+1}))^2] + \frac{3(\epsilon - \sigma)}{\tau\bar{\mu}} \mathbb{E}[\Gamma_{k+1} - \Gamma_k].$$

Summing up from $k = 1$ to K , we can conclude that

$$\mathbb{E}[\Psi_1 - \Psi_{K+1}] \geq \frac{\epsilon - \sigma}{\bar{\mu}} \sum_{k=1}^K \mathbb{E}[\text{dist}(0, \partial\Phi(A^{k+1}))^2] + \frac{3(\epsilon - \sigma)}{\tau\bar{\mu}} \mathbb{E}[\Gamma_{K+1} - \Gamma_1],$$

implying the existence of $\hat{k} \in 2, \dots, K + 1$ such that

$$\begin{aligned} \mathbb{E}[\text{dist}(0, \partial\Phi(A^{\hat{k}}))^2] &\leq \frac{1}{K} \sum_{k=1}^K \mathbb{E}[\text{dist}(0, \partial\Phi(A^{k+1}))^2] \\ &\leq \frac{\bar{\mu}}{(\epsilon - \sigma)K} (\mathbb{E}[\Psi_1 - \Psi_{K+1}] + \frac{3(\epsilon - \sigma)}{\tau\bar{\mu}} \mathbb{E}[\Gamma_1 - \Gamma_{K+1}]) \\ &\leq \frac{\bar{\mu}}{(\epsilon - \sigma)K} (\mathbb{E}\Psi_1 + \frac{3(\epsilon - \sigma)}{\tau\bar{\mu}} \mathbb{E}\Gamma_1). \end{aligned}$$

The proof is completed. \square

Define the set of limit points of $\{A^k\}_{k \in \mathbb{N}}$ as

$$\Omega(A^0) := \{A^* : \exists \text{ an increasing sequence of integers } \{k_l\}_{l \in \mathbb{N}} \text{ such that } A^{k_l} \rightarrow A^* \text{ as } l \rightarrow +\infty\}.$$

Next, by combining Theorems 1 and 2 with the KL property [3, 12], we are ready to outline the global convergence result for the Midas-LL1 algorithm in the following theorem. The proof details are omitted here for brevity, but readers may refer to [12, 44].

Theorem 3. *Suppose that Assumption 1 is satisfied, the step η_k is within the range $[\underline{\eta}, \bar{\eta}]$ and (28) is satisfied. Let the sequence $\{A^k\}_{k \in \mathbb{N}}$ generated by Algorithm 1 with variance-reduced gradient estimator be bounded, where $A^k = \{A_1^k, A_2^k, A_3^k\}$. Φ is a semialgebraic function that satisfies the KL property with exponent $\theta \in [0, 1)$, then either the point A^k reaches a critical point after a finite number of iterations or the sequence $\{A^k\}_{k \in \mathbb{N}}$ almost surely demonstrates the finite length property in expectation,*

$$\sum_{k=0}^{+\infty} \mathbb{E}\|A^{k+1} - A^k\|_F < +\infty.$$

5 Numerical experiments

In this section, we present the effectiveness of the proposed Midas-LL1 (Algorithm 1) through numerical experiments conducted on two real-world hyperspectral sub-image (HSI) datasets¹, Salinas and Pavia, and two video datasets, Carphone and Foreman. We aim to demonstrate its superior efficiency through comparisons with the state-of-the-art algorithm ALS-MU-based LL1 algorithms,

¹http://www.ehu.es/ccwintco/index.php/Hyperspectral_Remote_Sensing_Scenes.

namely, MVNTF in [37], which also does not have any structural regularization on the factors except for the nonnegativity constraints.

To evaluate its performance, Midas-LL1 is implemented with three stochastic gradient estimators: vanilla SGD, the unbiased variance-reduced SAGA [10], and the biased variance-reduced SARAH [32]. This study facilitates a comparative analysis of gradient bias properties and variance reduction strategies. Additionally, we consider multi-step inertial acceleration with $t = 3$, one-step inertial acceleration with $t = 1$, and also no acceleration version with $t = 0$, respectively. The combinations of these stochastic gradient estimators and multi-step inertial acceleration schemes are denoted as 3-Midas-SGD/SAGA/SARAH, 1-Midas-SGD/SAGA/SARAH, and 0-Midas-SGD/SAGA/SARAH, respectively.

Because the proposed algorithms under test involve different operations and subproblem-solving strategies, finding a unified complexity measure can be challenging, especially with multi-step acceleration that varies with different t . To address this issue, all algorithms are run for a fixed 200 epochs, and we present the final outcomes obtained. When handling large-scale tensor decomposition problems in video dataset experiments, the MVNTF algorithms typically run with extra lengthy time, yet fail to meet the specified stopping criterion. In this case, we set the maximal number of iterations to be 1000. Additionally, we evaluate the cost value of the algorithms about runtime, providing a comprehensive comparison of performance.

In all experiments, we set $L_r = L$, for $r = 1, \dots, R$, stepsize $\eta^k = \eta = 0.1$, the batchsize of sampled fibers $B = 2L$, the inertial parameters $\alpha^k = 0.3 \times \frac{k-1}{k+2}$ and $\beta^k = 0.8 \times \frac{k-1}{k+2}$.

The peak signal-to-noise ratio (PSNR) values are considered to measure the numerical performance for the real dataset experiments. The PSNR value is defined as

$$\text{PSNR} = 10 \log_{10} \left(\frac{\mathcal{X}_{\max}^2 \prod_{i=1}^N I_i}{\|\mathcal{X} - \bar{\mathcal{X}}\|_F^2} \right),$$

where \mathcal{X}_{\max} is the maximum intensity of the original dataset \mathcal{X} and $\bar{\mathcal{X}} = \sum_{r=1}^R (A_{1,r} \cdot A_{2,r}^\top) \circ \mathbf{c}_r$ denotes the rank- $(L, L, 1)$ BTD approximation of \mathcal{X} . We also adopt cross correlation (CC), root mean square error (RMSE), spectral angle mapper (SAM) to illustrate the stability of all algorithms.

5.1 Comparisons of zero-step, one-step, and three-step Midas-LL1

In this subsection, we present the performance of various methods on hyperspectral sub-image datasets (dimensions: height \times width \times bands) to compare the effectiveness of Midas-LL1 with zero-step, one-step, and three-step accelerations. Hyperspectral images (HSI) capture both spatial and spectral information by recording reflectance values across multiple wavelengths, making them a valuable tool for applications such as remote sensing and material classification. The spectral-spatial joint structure of HSI is naturally suited for Midas-LL1 algorithms because rank- $(L_r, L_r, 1)$ block-term decomposition provides a particularly effective framework for modeling this structure. The datasets used for the experiments include Salinas ($80 \times 84 \times 204$), which focuses on agricultural regions, and Pavia Centre ($288 \times 352 \times 300$), which captures an urban environment with intricate spatial patterns.

5.1.1 Salinas

We first present the numerical experiments on Salinas dataset with different values of R and L in Figure 5. Midas-LL1 with multi-step acceleration ($t = 3$) outperforms both one-step ($t = 1$) and zero-step ($t = 0$) methods. This confirms the effectiveness of our proposed multi-step inertial accelerated method in solving the tensor BTD problem. Notably, Midas-LL1 with the variance-reduced SGD estimator outperforms Midas-LL1 with the vanilla SGD estimator in three-step, one-step, and zero-step settings, with the latter two showing even more pronounced improvements.

We continue to show the final performance of the return tensor in terms of RMSE, SAM, CC, and PSNR in Table 1. From the results, we see that both 3-Midas-SAGA and 3-Midas-SARAH achieve superior performance, demonstrating that variance-reduced stochastic gradient estimators effectively enhance reconstruction accuracy. Their consistent performance across different configurations of R and L further highlights the stability and adaptability of these methods for hyperspectral image data.

The rank- $(L_r, L_r, 1)$ block-term tensor decomposition approximation results for the Salinas dataset are shown in Figures 6. These results demonstrate that the proposed Midas-LL1 method with multi-step acceleration ($t = 3$) surpasses both one-step ($t = 1$) and zero-step ($t = 0$) methods in recovering the original Salinas dataset, as illustrated in Figure 6 with varying R and L . Furthermore, methods employing SAGA and SARAH stochastic gradient estimators consistently achieve better performance compared to those based on SGD, particularly in producing clearer boundaries between different regions in the images.

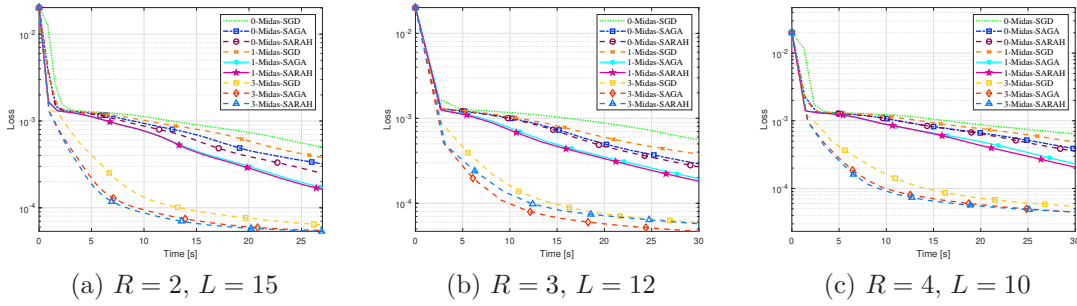


Figure 5: Numerical experiments on the $80 \times 84 \times 204$ Salinas dataset with different values of R and L .

Table 1: Comparisons of Midas-LL1 with zero-step, one-step, and three-step inertial acceleration on Salinas dataset. The parameters $\alpha^k = 0.3 \times \frac{k-1}{k+2}$, $\beta^k = 0.8 \times \frac{k-1}{k+2}$, and $\eta^k = 0.1$. “ a_0 ” denotes 0-Midas-SGD; “ a_1 ” denotes 0-Midas-SAGA; “ a_2 ” denotes 0-Midas-SARAH; “ b_0 ” denotes 1-Midas-SGD; “ b_1 ” denotes 1-Midas-SAGA; “ b_2 ” denotes 1-Midas-SARAH; “ c_0 ” denotes 3-Midas-SGD; “ c_1 ” denotes 3-Midas-SAGA; “ c_2 ” denotes 3-Midas-SARAH.

R	L	Index	a_0	a_1	a_2	b_0	b_1	b_2	c_0	c_1	c_2
2	15	RMSE (0)	0.0413	0.0211	0.0210	0.0247	0.0151	0.0150	0.0109	0.0101	0.0101
		SAM (0)	0.1585	0.0718	0.0716	0.0864	0.0524	0.0523	0.0406	0.0382	0.0379
		CC (1)	0.1153	0.8178	0.8191	0.7328	0.8977	0.8985	0.9269	0.9346	0.9354
		PSNR (∞)	27.676	33.528	33.543	32.147	36.440	36.483	39.231	39.934	39.946
3	12	RMSE (0)	0.0281	0.0197	0.0195	0.0225	0.0152	0.0153	0.0101	0.0087	0.0093
		SAM (0)	0.0969	0.0676	0.0669	0.0767	0.0527	0.0532	0.0392	0.0346	0.0359
		CC (1)	0.6063	0.8235	0.8273	0.7676	0.8851	0.8843	0.9309	0.9438	0.9433
		PSNR (∞)	31.021	34.103	34.207	36.360	38.814	36.333	39.886	41.218	40.644
4	10	RMSE (0)	0.0277	0.0175	0.0175	0.0193	0.0133	0.0132	0.0090	0.0083	0.0082
		SAM (0)	0.1002	0.0620	0.0626	0.0685	0.0479	0.0479	0.0350	0.0326	0.0331
		CC (1)	0.5754	0.8625	0.8628	0.8399	0.9071	0.9072	0.9446	0.9513	0.9500
		PSNR (∞)	31.144	35.145	35.115	34.283	37.549	37.579	40.877	41.606	41.715

5.1.2 Pavia Centre

Next, we analyze the performance of the algorithms on the Pavia Centre dataset, and the results are presented in Figure 7 and Table 2. Again, compared with Midas-LL1 Methods with one-step or

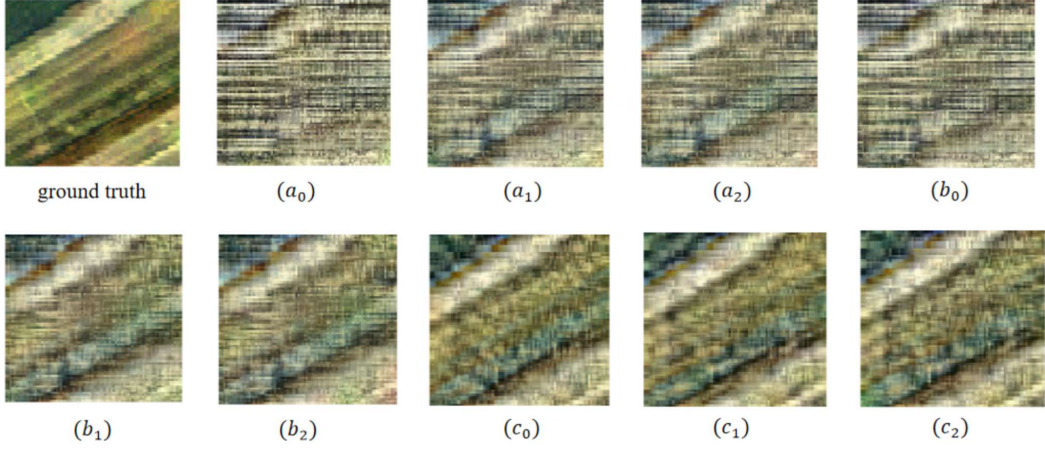


Figure 6: The results of Midas-LL1 for rank- $(L_r, L_r, 1)$ block-term tensor decomposition approximation on the 15-th frame of the *Salinas* dataset with $R = 3$ and $L = 12$. “ a_0 ” denotes 0-Midas-SGD; “ a_1 ” denotes 0-Midas-SAGA; “ a_2 ” denotes 0-Midas-SARAH; “ b_0 ” denotes 1-Midas-SGD; “ b_1 ” denotes 1-Midas-SAGA; “ b_2 ” denotes 1-Midas-SARAH; “ c_0 ” denotes 3-Midas-SGD; “ c_1 ” denotes 3-Midas-SAGA; “ c_2 ” denotes 3-Midas-SARAH.

zero-step acceleration, Midas-LL1 Methods with three-step acceleration (3-Midas-SGD, 3-Midas-SAGA, 3-Midas-SARAH) demonstrate the fastest convergence and achieve the lowest loss across all configurations of R and L , indicating the effectiveness of multi-step acceleration in improving performance. Among the three-step methods, 3-Midas-SAGA and 3-Midas-SARAH consistently outperform 3-Midas-SGD in terms of both convergence speed and final loss, highlighting the advantages of variance reduction techniques.

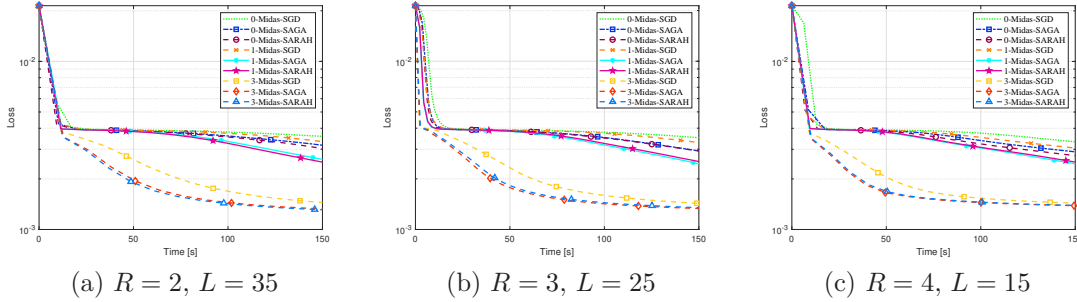


Figure 7: Numerical experiments on the $610 \times 340 \times 103$ Pavia Centre dataset with different values of R and L .

Table 2: Comparisons of Midas-LL1 with zero-step, one-step, and three-step inertial acceleration on Pavia Centre dataset. The parameters $\alpha^k = 0.3 \times \frac{k-1}{k+2}$, $\beta^k = 0.8 \times \frac{k-1}{k+2}$, and $\eta^k = 0.1$. “ a_0 ” denotes 0-Midas-SGD; “ a_1 ” denotes 0-Midas-SAGA; “ a_2 ” denotes 0-Midas-SARAH; “ b_0 ” denotes 1-Midas-SGD; “ b_1 ” denotes 1-Midas-SAGA; “ b_2 ” denotes 1-Midas-SARAH; “ c_0 ” denotes 3-Midas-SGD; “ c_1 ” denotes 3-Midas-SAGA; “ c_2 ” denotes 3-Midas-SARAH.

R	L	Index	a_0	a_1	a_2	b_0	b_1	b_2	c_0	c_1	c_2
2	35	RMSE (0)	0.0739	0.0610	0.0603	0.0627	0.0540	0.0539	0.0503	0.0491	0.0491
		SAM (0)	0.2453	0.2041	0.1999	0.2071	0.1685	0.1684	0.1534	0.1501	0.1500
		CC (1)	0.5951	0.7431	0.7501	0.7277	0.8058	0.8060	0.8328	0.8401	0.8402
		PSNR (∞)	22.626	24.294	24.397	24.056	25.358	25.360	25.976	26.180	26.177
3	25	RMSE (0)	0.0676	0.0550	0.0552	0.0571	0.0517	0.0518	0.0503	0.0492	0.0495
		SAM (0)	0.2265	0.1761	0.1764	0.1843	0.1650	0.1648	0.1596	0.1586	0.1586
		CC (1)	0.6745	0.7995	0.7985	0.7823	0.8248	0.8246	0.8261	0.8349	0.8323
		PSNR (∞)	23.401	25.188	25.168	24.871	25.724	25.716	25.970	26.158	26.111
4	15	RMSE (0)	0.0611	0.0555	0.0555	0.0561	0.0528	0.0528	0.0510	0.0503	0.0508
		SAM (0)	0.1902	0.1744	0.1746	0.1757	0.1635	0.1636	0.1557	0.1536	0.1561
		CC (1)	0.7409	0.7904	0.7903	0.7867	0.8126	0.8126	0.8258	0.8308	0.8274
		PSNR (∞)	24.285	25.116	25.109	25.028	25.550	25.547	25.854	25.976	25.891

5.2 Comparing Midas-LL1 under one-step and three-step acceleration with MVNTF.

In this subsection, we evaluate two video datasets² (with dimensions: length \times width \times frames) to compare the performance of Midas-LL1 under one-step and three-step acceleration with MVNTF. The datasets used for testing include Carphone ($144 \times 176 \times 396$) and Foreman ($288 \times 352 \times 300$). These video datasets, collected and maintained by Arizona State University, are widely used in research.

5.2.1 Carphone

We evaluate the algorithms on the Carphone dataset, terminating all runs at 80 seconds, and present the results in Figure 8. The performance of the three Midas-LL1 methods with $t = 3$, namely 3-Midas-SGD, 3-Midas-SAGA, and 3-Midas-SARAH, consistently outperforms MVNTF and one-step Midas-LL1 methods from $R = 3$ to $R = 5$. For $R = 3$ and $L = 2$, the one-step accelerated methods with $t = 1$ also outperform MVNTF. However, as R increases, 1-Midas-SGD only demonstrates a very slight improvement over MVNTF, shown in Figure 8 (c), while 1-Midas-SAGA and 1-Midas-SARAH exhibit stable performance, highlighting the effectiveness of variance-reduced stochastic gradient estimators.

We continue to show the final performance of the return tensor in terms of RMSE, SAM, CC, and PSNR in Table 3. The results show that 3-Midas-SARAH demonstrates robustness in reconstructing and preserving both spatial and spectral information across various settings. However, when $R = 4$, 3-Midas-SGD achieves superior performance. This result highlights that the potential advantage of the vanilla SGD approach.

5.2.2 Foreman

Finally, we analyze the algorithms on the Foreman video dataset in Figure 9 and Table 4. As R increases, the performance gap between MVNTF and Midas-LL1 widens, with three-step acceleration methods (3-Midas-SGD, 3-Midas-SAGA, 3-Midas-SARAH) consistently demonstrating superiority. Particularly, variance-reduced estimators SAGA and SARAH achieve faster convergence and lower loss across all configurations, outperforming MVNTF and one-step methods, especially under

²<http://trace.eas.asu.edu/yuv/>

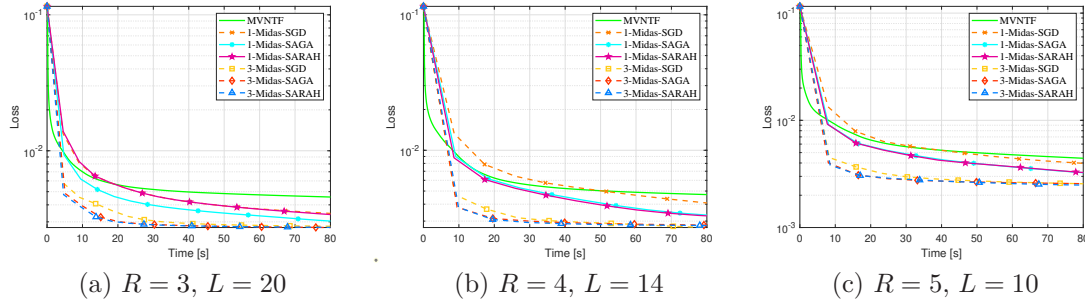


Figure 8: Numerical experiments of Midas-LL1 under 1-step and 3-step acceleration with MVNTF on the $144 \times 176 \times 396$ Carphone dataset.

Table 3: Comparisons of Midas-LL1 under one-step and three-step inertial acceleration with MVNTF on Carphone dataset. The parameters $\alpha^k = 0.3 \times \frac{k-1}{k+2}$, $\beta^k = 0.8 \times \frac{k-1}{k+2}$, and $\eta^k = 0.1$. “a” denotes MVNTF; “ b_0 ” denotes 1-Midas-SGD; “ b_1 ” denotes 1-Midas-SAGA; “ b_2 ” denotes 1-Midas-SARAH; “ c_0 ” denotes 3-Midas-SGD; “ c_1 ” denotes 3-Midas-SAGA; “ c_2 ” denotes 3-Midas-SARAH.

Dataset	R	L	Index	a	b_0	b_1	b_2	c_0	c_1	c_2
<i>Carphone</i>	3	20	RMSE (0)	0.0877	0.0819	0.0765	0.0750	0.0744	0.0736	0.0732
			SAM (0)	0.2175	0.2071	0.1862	0.1792	0.1779	0.1751	0.1745
			CC (1)	0.9444	0.9514	0.9577	0.9595	0.9600	0.9609	0.9613
			PSNR (∞)	21.136	21.735	22.321	22.502	22.566	22.660	22.707
	4	14	RMSE (0)	0.0941	0.0821	0.0776	0.0776	0.0718	0.0737	0.0739
			SAM (0)	0.2391	0.2003	0.1914	0.1916	0.1802	0.1813	0.1810
			CC (1)	0.9357	0.9513	0.9566	0.9566	0.9630	0.9609	0.9607
			PSNR (∞)	21.072	22.262	22.749	22.747	23.419	23.194	23.174
	5	10	RMSE (0)	0.0939	0.0779	0.0745	0.0746	0.0698	0.0698	0.0693
			SAM (0)	0.2294	0.1802	0.1731	0.1719	0.1704	0.1708	0.1648
			CC (1)	0.9356	0.9560	0.9598	0.9597	0.9649	0.9650	0.9654
			PSNR (∞)	20.544	22.165	22.554	22.542	23.117	23.120	23.184

larger R and L settings. This trend indicates that Midas-LL1 is better suited for higher numbers of components R in rank- $(L_r, L_r, 1)$ block-term tensor decomposition. While one-step methods (1-Midas-SGD, 1-Midas-SAGA, 1-Midas-SARAH) perform moderately well, they exhibit higher loss compared to three-step methods.

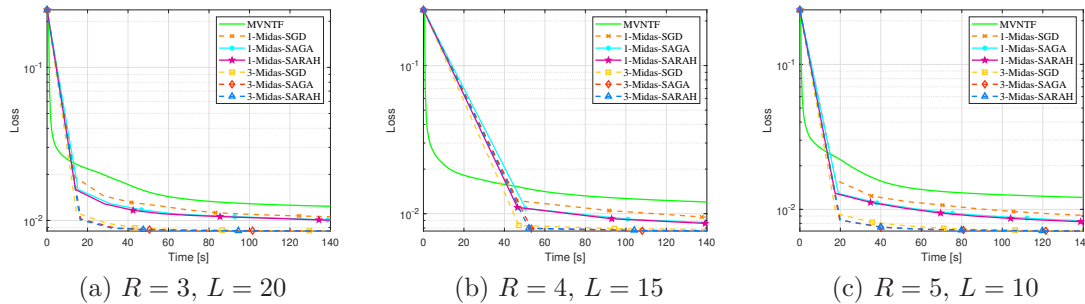


Figure 9: Numerical experiments of Midas-LL1 under 1-step and 3-step acceleration with MVNTF on the $288 \times 352 \times 300$ Foreman dataset.

Table 4: Comparisons of Midas-LL1 under one-step and three-step inertial acceleration with MVNTF on Foreman dataset. The parameters $\alpha^k = 0.3 \times \frac{k-1}{k+2}$, $\beta^k = 0.8 \times \frac{k-1}{k+2}$, and $\eta^k = 0.1$. “a” denotes MVNTF; “ b_0 ” denotes 1-Midas-SGD; “ b_1 ” denotes 1-Midas-SAGA; “ b_2 ” denotes 1-Midas-SARAH; “ c_0 ” denotes 3-Midas-SGD; “ c_1 ” denotes 3-Midas-SAGA; “ c_2 ” denotes 3-Midas-SARAH.

Dataset	R	L	Index	a	b_0	b_1	b_2	c_0	c_1	c_2
Foreman	3	20	RMSE (0)	0.1530	0.1381	0.1318	0.1317	0.1305	0.1305	0.1304
			SAM (0)	0.2403	0.2167	0.2069	0.2067	0.2046	0.2045	0.2047
			CC (1)	0.7914	0.8306	0.8468	0.8469	0.8500	0.8501	0.8503
			PSNR (∞)	16.306	17.197	17.601	17.605	17.690	17.690	17.691
	4	15	RMSE (0)	0.1465	0.1292	0.1265	0.1265	0.1233	0.1228	0.1228
			SAM (0)	0.2273	0.2012	0.1977	0.1977	0.1946	0.1936	0.1938
			CC (1)	0.8051	0.8527	0.8597	0.8597	0.8675	0.8688	0.8689
			PSNR (∞)	16.686	17.776	17.961	17.959	18.181	18.219	18.219
	5	10	RMSE (0)	0.1457	0.1246	0.1221	0.1197	0.1186	0.1186	0.1187
			SAM (0)	0.2261	0.1958	0.1916	0.1885	0.1871	0.1870	0.1873
			CC (1)	0.8075	0.8641	0.8696	0.8755	0.8782	0.8783	0.8780
			PSNR (∞)	16.730	18.090	18.267	18.439	18.518	18.518	18.508

6 Conclusion

In this paper, we proposed Midas-LL1, a multi-step inertial accelerated block-randomized stochastic gradient descent method designed for the rank- $(L_r, L_r, 1)$ block-term tensor decomposition problem. Leveraging an extended multi-step and multi-block variance-reduced stochastic estimator, we demonstrated that the proposed algorithm achieves a sublinear convergence rate for the generated subsequence. Furthermore, we established the global convergence of the sequence generated by Midas-LL1 using a novel multi-step Lyapunov function, proving that the algorithm requires at most $\mathcal{O}(\varepsilon^{-2})$ iterations in expectation to reach an ε -stationary point. Extensive experiments on synthetic and real-world datasets validated the effectiveness of Midas-LL1, demonstrating its superior convergence behavior with multi-step inertial acceleration compared to one-step methods and existing algorithms. The results highlight the advantages of the proposed multi-step approach in achieving better performance and faster convergence.

Declarations

Funding: This research is supported by the National Natural Science Foundation of China (NSFC) grant 12401415, 12471282, 12171021, the R&D project of Pazhou Lab (Huangpu) (Grant no. 2023K0603), and the Fundamental Research Funds for the Central Universities (Grant No. YWF-22-T-204).

Competing interests: The authors have no competing interests to declare that are relevant to the content of this article.

Data Availability Statement: Data will be made available on reasonable request.

References

- [1] A. Auslender. Asymptotic properties of the fenchel dual functional and applications to decomposition problems. *J. Optim. Theory Appl.*, 73(3):427–449, 1992.
- [2] J. M. Bioucas-Dias et al. Hyperspectral unmixing overview: Geometrical, statistical, and sparse regression-based approaches. *IEEE J. Sel. Topics Appl. Earth Observ. Remote Sens.*, 5(2):354–379, Apr 2012.

- [3] J. Bolte, S. Sabach, and M. Teboulle. Proximal alternating linearized minimization for non-convex and nonsmooth problems. *Math. Program.*, 146(1-2):459–494, 2014.
- [4] J. Bolte, S. Sabach, M. Teboulle, and Y. Vaisbourd. First order methods beyond convexity and Lipschitz gradient continuity with applications to quadratic inverse problems. *SIAM J. Optim.*, 28(3):2131–2151, 2018.
- [5] M. Che and Y. Wei. Multiplicative algorithms for symmetric nonnegative tensor factorizations and its applications. *J. Sci. Comput.*, 83(3):53, 2020.
- [6] P. Comon, G. H. Golub, L. Lim, and B. Mourrain. Symmetric tensors and symmetric tensor rank. *SIAM J. Matrix Anal. Appl.*, 30(3):1254–1279, 2008.
- [7] L. De Lathauwer. Decompositions of a higher-order tensor in block terms—part I: Lemmas for partitioned matrices. *SIAM J. Matrix Anal. Appl.*, 30(3):1022–1032, 2008.
- [8] L. De Lathauwer. Decompositions of a higher-order tensor in block terms—part II: Definitions and uniqueness. *SIAM J. Matrix Anal. Appl.*, 30(3):1033–1066, 2008.
- [9] L. De Lathauwer and D. Nion. Decompositions of a higher-order tensor in block terms—part III: Alternating least squares algorithms. *SIAM J. Matrix Anal. Appl.*, 30(3):1067–1083, 2008.
- [10] A. Defazio, F. R. Bach, and S. Lacoste-Julien. SAGA: A fast incremental gradient method with support for non-strongly convex composite objectives. In *Advances in Neural Information Processing Systems 27*, pages 1646–1654, 2014.
- [11] I. Domanov, N. Vervliet, E. Evert, and L. De Lathauwer. Decomposition of a tensor into multilinear rank- (M_r, N_r, \cdot) terms. *SIAM Journal on Matrix Analysis and Applications*, 45(3):1310–1334, 2024.
- [12] D. Driggs, J. Tang, J. Liang, M. E. Davies, and C. Schönlieb. A stochastic proximal alternating minimization for nonsmooth and nonconvex optimization. *SIAM J. Imaging Sci.*, 14(4):1932–1970, 2021.
- [13] X. Fu and K. Huang. Block-term tensor decomposition via constrained matrix factorization. In *Proc. Mach. Learn. Signal Process.*, Oct 2019.
- [14] X. Fu, S. Ibrahim, H. Wai, C. Gao, and K. Huang. Block-randomized stochastic proximal gradient for low-rank tensor factorization. *IEEE Trans. Signal Process.*, 68:2170–2185, 2020.
- [15] N. Gillis and F. Glineur. Accelerated multiplicative updates and hierarchical als algorithms for nonnegative matrix factorization. *Neural Comput.*, 24(4):1085–1105, 2012.
- [16] E. Gujral, R. Pasricha, and E. E. Papalexakis. Beyond rank-1: Discovering rich community structure in multi-aspect graphs. In *Proc. WWW-2020*, Apr 2020.
- [17] C. Guo, J. Zhao, and Q. L. Dong. A stochastic two-step inertial bregman proximal alternating linearized minimization algorithm for nonconvex and nonsmooth problems. *Numer. Algor.*, 2023.
- [18] J. Hertrich and G. Steidl. Inertial stochastic PALM and applications in machine learning. *Sampl. Theory Signal Process. Data Anal.*, 20(1), 2022.
- [19] F. L. Hitchcock. The expression of a tensor or a polyadic as a sum of products. *J. Math. Phys.*, 6(1-4):164–189, 1927.

- [20] F. L. Hitchcock. Multiple invariants and generalized rank of a p-way matrix or tensor. *J. Math. Phys.*, 7(1-4):39–79, 1928.
- [21] D. Hong, T. G. Kolda, and J. A. Duersch. Generalized canonical polyadic tensor decomposition. *SIAM Rev.*, 62(1):133–163, 2020.
- [22] C. Jutten and J. Herault. Blind separation of sources, part i: An adaptive algorithm based on neuromimetic architecture. *Signal Process.*, 24(1):1–10, 1991.
- [23] T. G. Kolda and B. W. Bader. Tensor decompositions and applications. *SIAM Rev.*, 51(3):455–500, 2009.
- [24] W. P. Krijnen, T. K. Dijkstra, and A. Stegeman. On the non-existence of optimal solutions and the occurrence of "degeneracy" in the CANDECOMP/PARAFAC model. *Psychometrika*, 73(3):431–439, 2008.
- [25] G. Lan. *First-Order and Stochastic Optimization Methods for Machine Learning*. Springer, 2020.
- [26] D. D. Lee and H. S. Seung. Algorithms for non-negative matrix factorization. In *Proc. Int. Conf. Neural Inf. Process. Syst.*, pages 556–562, 2001.
- [27] J. Liang, J. Fadili, and G. Peyré. A multi-step inertial forward–backward splitting method for non-convex optimization, 2016.
- [28] L.-H. Lim and P. Comon. Nonnegative approximations of nonnegative tensors. *J. Chemom.*, 23:432–441, 2009.
- [29] C.-J. Lin. On the convergence of multiplicative update algorithms for nonnegative matrix factorization. *IEEE Trans. Neural Netw.*, 18(6):1589–1596, 2007.
- [30] Z. Liu, Q. Wang, C. Cui, and Y. Xia. Inertial accelerated stochastic mirror descent for large-scale generalized tensor cp decomposition, 2024.
- [31] W. Ma et al. A signal processing perspective on hyperspectral unmixing: Insights from remote sensing. *IEEE Signal Process. Mag.*, 31(1):67–81, Jan 2014.
- [32] L. M. Nguyen, J. Liu, K. Scheinberg, and M. Takác. SARAH: A novel method for machine learning problems using stochastic recursive gradient. In *Proceedings of the 34th International Conference on Machine Learning*, pages 2613–2621, 2017.
- [33] P. Paatero. Construction and analysis of degenerate PARAFAC models. *J. Chemom.*, 14(3):285–299, 2000.
- [34] T. Pock and S. Sabach. Inertial proximal alternating linearized minimization (iPALM) for nonconvex and nonsmooth problems. *SIAM J. Imaging Sci.*, 9(4):1756–1787, 2016.
- [35] B. T. Polyak. Some methods of speeding up the convergence of iteration methods. *USSR Comput. Math. Math. Phys.*, 4(5):1–17, 1964.
- [36] W. Pu, S. Ibrahim, X. Fu, and M. Hong. Stochastic mirror descent for low-rank tensor decomposition under non-euclidean losses. *IEEE Trans. Signal Process.*, 70:1803–1818, 2022.
- [37] Y. Qian, F. Xiong, S. Zeng, J. Zhou, and Y. Y. Tang. Matrix-vector nonnegative tensor factorization for blind unmixing of hyperspectral imagery. *IEEE Trans. Geosci. Remote Sens.*, 55(3):1776–1792, Mar 2017.

- [38] R. T. Rockafellar and R. J.-B. Wets. *Variational Analysis*. Grundlehren der Mathematischen Wissenschaften, 317, Springer, 1998.
- [39] P. Tseng. Convergence of a block coordinate descent method for nondifferentiable minimization. *J. Optim. Theory Appl.*, 109:475–494, 2001.
- [40] L. R. Tucker. Implications of factor analysis of three-way matrices for measurement of change. *Probl. Meas. Change*, 15:122–137, 1963.
- [41] L. R. Tucker. Some mathematical notes on three-mode factor analysis. *Psychometrika*, 31(3):279–311, 1966.
- [42] L. R. Tucker et al. The extension of factor analysis to three-dimensional matrices. *Contrib. Math. Psychol.*, pages 110–119, 1964.
- [43] Q. Wang, C. Cui, and D. Han. A momentum block-randomized stochastic algorithm for low-rank tensor CP decomposition. *Pac. J. Optim.*, 17(3):433–452, 2021.
- [44] Q. Wang and D. Han. A Bregman stochastic method for nonconvex nonsmooth problem beyond global Lipschitz gradient continuity. *Optim. Methods. Softw.*, 38(5):914–946, 2023.
- [45] Q. Wang, Z. Liu, C. Cui, and D. Han. Inertial accelerated sgd algorithms for solving large-scale lower-rank tensor CP decomposition problems. *J. Comput. Appl. Math.*, 423:114948, 2023.
- [46] Q. Wang, Z. Liu, C. Cui, and D. Han. A Bregman proximal stochastic gradient method with extrapolation for nonconvex nonsmooth problems. In *AAAI Conf. Artif. Intell.*, volume 38, pages 15580–15588, 2024.
- [47] F. Xiong, Y. Qian, J. Zhou, and Y. Y. Tang. Hyperspectral unmixing via total variation regularized nonnegative tensor factorization. *IEEE Trans. Geosci. Remote Sens.*, 57(4):2341–2357, 2019.
- [48] Y. Xu and W. Yin. A block coordinate descent method for regularized multiconvex optimization with applications to nonnegative tensor factorization and completion. *SIAM J. Imag. Sci.*, 6(3):1758–1789, 2013.
- [49] Y. Xu and W. Yin. Block stochastic gradient iteration for convex and nonconvex optimization. *SIAM J. Optim.*, 25(3):1686–1716, 2015.